Effects of winds and Caribbean eddies on the frequency of Loop Current eddy shedding: A numerical model study

L.-Y. Oey and H.-C. Lee
Princeton University, Princeton, New Jersey, USA

William J. Schmitz Jr.
Conrad Blucher Institute, Texas A&M University, Corpus Christi, Texas, USA

Received 31 October 2002; revised 16 June 2003; accepted 17 July 2003; published 16 October 2003.

[1] The Loop Current (LC) is known to shed eddies at irregular intervals from 3 to 17 months. The causes of this irregularity have not, however, been adequately identified previously. We examine the effects of various types of external forcing on shedding with a model of the western North Atlantic Ocean (96°–55°W, 6°–50°N). We force the model with steady transport at 55°W, with winds, and include eddies in the Caribbean Sea. We examine their separate effects. With steady transport only, the model sheds rings at a dominant period of 9–10 months. Wind-induced transport fluctuations through the Greater Antilles Passages cause shedding at shorter intervals (≈3–7 months). Caribbean eddies (anticyclones) cause shedding at longer periods (≈14–16 months). Potential vorticity conservation indicates that Caribbean eddies tend to deter northward extension of the LC into the Gulf, which can lead to longer periods between eddy shedding. Fluctuating inflow at the Yucatan Channel that is associated with winds and/or Caribbean eddies can cause an LC eddy to temporarily (∼1 month) detach from and then reattach back to the LC, a phenomenon often observed. Model results also suggest that southwest of Hispaniola, warm eddies are spun up by the local wind stress curl. This type of eddy drifts southwestward, then westward after merging with the Caribbean Current, and then northward as it progresses toward the Yucatan Channel; these eddies significantly affect the shedding behavior of warm-core rings. The timescale for spin up and drift from Hispaniola is about 100 days. Satellite data indicate the existence of these eddies in the real ocean. *INDEX TERMS:* 4520 Oceanography: Physical: Eddies and mesoscale processes; 4255 Oceanography: General: Numerical modeling; 4243 Oceanography: General: Marginal and semienclosed seas; 4576 Oceanography: Physical: Western boundary currents; 4512 Oceanography: Physical: Currents; *KEYWORDS:* Gulf of Mexico, Caribbean Current, Loop Current, eddy shedding, winds and eddies, numerical ocean model

Citation: Oey, L.-Y., H.-C. Lee, and W. J. Schmitz Jr., Effects of winds and Caribbean eddies on the frequency of Loop Current eddy shedding: A numerical model study, *J. Geophys. Res.*, *108*(C10), 3324, doi:10.1029/2002JC001698, 2003.

1. Introduction

[2] Currents through the Caribbean Sea, the Gulf of Mexico, and the Florida Straits constitute an important component of the subtropical gyre circulation of the North Atlantic Ocean. This fact is vividly presented by *Fratantoni*'s [2001] decadal, quasi-Eulerian mean drifter analysis. The author's Plate 6, for example, shows dominant speeds in the Caribbean Current (>0.5 m s^{-1}) in the southern portion of the Caribbean Sea, the Loop Current (LC), and Florida Current (both >1 m s^{-1}). Figure 1 gives an example of the regional, near-surface circulation taken from a separate study by L.-Y. Oey et al. (manuscript in preparation, 2003, hereinafter referred to as Oey et al., manuscript in preparation, 2003). These authors combined satellite sea surface height (SSH) anomaly data from the work of *Ducet et al.* [2000] with an Ocean General Circulation Model (OCGM). The figure also gives the nomenclatures and acronyms that we will use throughout the paper. In this quasi-synoptic picture (Figure 1 is for 19–28 July 1997), one can see complex patterns of currents and eddies at several space scales. The Loop Current, for example, is in the process of shedding a Loop Current eddy (LCE), and appears to be "cleaved" by a cyclone off the west Florida slope. Though details differ, such cleavage of the Loop Current appears to be quite a common phenomenon and was first noted more than three decades ago by *Cochrane* [1972] [also see the work of *Vukovich and Maul*, 1985]. There are other, smaller eddies in the Gulf, including an older LCE in the northwestern Gulf. (The existence of smaller cyclonic eddies in the western Gulf was noted in observations by *Merrell and Morrison* [1981] and *Brooks and Legeckis* [1982], but their abundance has only been more recently recognized when satellite and

0148-0227/03/2002JC001698$09.00

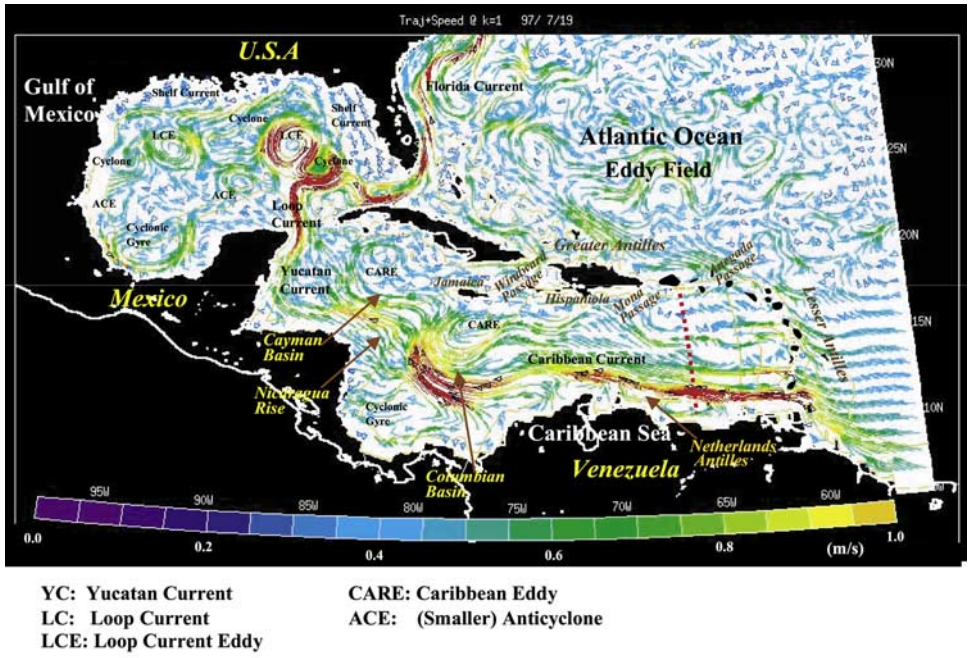

Figure 1. An example of the regional, near-surface circulation obtained by combining satellite SSH anomaly data from the work of *Ducet et al.* [2000] with an OCGM [*Oey et al.*, 2003]. Plotted are 10-day Eulerian trajectories $\mathbf{x} = \mathbf{x}_0 + \int \mathbf{u} dt$, where **x** and **u** are position and velocity vectors, respectively, and the integration is over 10 days. The trajectories are launched from 19 through 28 July 1997 and from every eighth grid point at the first sigma level (i.e., surface). Colors indicate speeds such that greenish blue is $\approx$0.5 m s^{-1} and red is $\geq$1 m s^{-1}.

high-resolution field measurements are available [e.g., *Hamilton*, 1992; *Hamilton et al.*, 2002].) Maximum speeds in the Yucatan Channel, the Loop Current, and the newly shed LCE as computed by *Oey et al.* [2003] from Figure 1 are 1.5, 1.8, and 1.6 m s^{-1}, respectively. The largest speeds in an LCE as observed by *Forristal et al.* [1992] are in this range. As in the work of *Fratantoni* [2001; also *Wilson and Leaman*, 2000], the Caribbean/Yucatan Current stands out as the dominant feature in the Caribbean Sea. Off the coast of Venezuela and the Netherlands Antilles (the dotted section in Figure 1), the westward jet in Figure 1 has a maximum speed of 1.08 m s^{-1}. This speed may be compared to acoustic Doppler current profiler (ADCP) measurements at 20-m depth by *Hernández-Guerra and Joyce* [2000], which yielded a value of 0.85 m s^{-1}. *Parr* [1937], *Wust* [1963, 1964], and *Gordon* [1967] contain comparatively early descriptions and discussions of the circulation in the Caribbean Sea. Parr clearly identifies the Caribbean Current (e.g., his Figure 63). Gordon's surface dynamic topographic map (relative to 1200-kb level) is reproduced here in Figure 2. It also indicates the existence of the Caribbean Current. Moreover, both Parr's and Gordon's maps (Figure 2) show a number of eddy and meander features, which can also be seen in Figure 1. These are (1) an anticyclonic high south of (between) Hispaniola and Jamaica; (2) a cyclonic gyre in southern Columbian Basin, along with a weaker cyclonic eddy off the Venezuela coast (between 65°W and 70°W); and (3) an anticyclonic meander east of the Nicaragua Rise where flow speeds increase. Except for the weak cyclone off the Venezuela coast, these features are also seen in *Fratantoni*'s [2001] and *Wilson and Leaman*'s [2000] drifter data. Fratantoni's data shows the anticyclone south of Hispaniola and Jamaica.

[3] Figure 1 implies a linkage between the Gulf of Mexico and the Caribbean Sea. The figure suggests that the behavior of the Loop Current may depend on "upstream" conditions in the Caribbean Sea and perhaps also on flow transports from the Atlantic through the Greater and Lesser Antilles (LA) Passages. This paper investigates how these upstream forcing processes affect the shedding frequency of the Loop Current.

[4] It is well known that the Loop Current sheds eddies at irregular intervals [e.g., *Vukovich*, 1995, and references quoted therein]. *Sturges and Leben* [2000] analyzed 26 years of observations and concluded that the shedding periods range from 3 to 17 months. *Schmitz* [2002] emphasizes the nearly white limited bandwidth character of the data set published by Sturges and Leben. The shedding irregularity may be in part a local (i.e., in the vicinity of the Yucatan Channel) dynamical phenomenon [*Hurlburt*, 1986; *Oey*, 1996] or it could also be caused by Yucatan flow fluctuations. These fluctuations are in part caused by complex environmental forcings of varying frequencies from the Caribbean Sea and the Atlantic Ocean. There are no studies that systematically consider the effects of these forcing(s) on shedding irregularity. When forced by a constant transport at Yucatan, models of varying designs and complexity consistently yield a nearly constant period of eddy shedding. For example, with a reduced gravity model, *Hurlburt and Thompson* [1980] obtained a period of 9 months. *Sturges et al.* [1993] obtained a period of 7 months using the *z* level Bryan-Cox model, and *Oey* [1996] obtained a

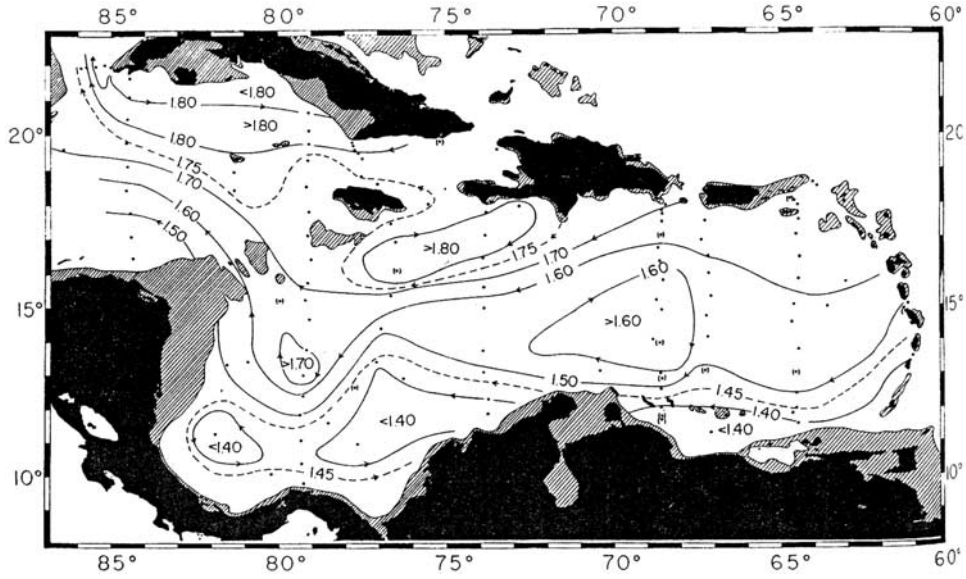

Figure 2. Sea surface dynamic topography relative to 1200-kb level (values in dynamic meters) [from *Gordon*, 1967].

period of 10 months using the sigma level Princeton Ocean Model (POM, his "experiment C1"). One possible exception was that Oey found irregular shedding even under constant transport when the horizontal viscosity was reduced (from values ≥ 50 m^2 s^{-1} commonly used in most early models). In this paper, we do not consider this possibility involving a "localized," natural chaotic behavior of the Loop Current. This requires a separate, full treatment, looking carefully also into the sensitivity of the solution to grid resolution at low viscosity, an extension of the work by *Oey* [1996].

[5] *Murphy et al.*'s [1999] model is forced by a combination of mean winds from the work of *Hellerman and Rosenstein* [1983] and wind fluctuations from the European Center for Medium-Range Weather Forecast (ECMWF). They show that Caribbean eddies that squeeze through the Yucatan Channel can affect the timing of shedding. The authors did not separate the eddy and wind effects. The Loop Current dynamics would depend on the ratio of channel width to R_0 (the first baroclinic Rossby radius) as well as the shears (i.e., R_0 itself). Murphy et al.'s horizontal resolution of 1/4° amounts to 5–8 points across the channel and is marginal in the Yucatan Channel, where $R_0 \approx 20$ km. (Their resolution should be adequate in the Caribbean Sea, the authors' main focus, where $R_0 \approx 40$–50 km). Nevertheless, the results presented by *Murphy et al.* [1999] suggest that Caribbean Sea dynamics may be important in the context of the eddy shedding behavior in the Loop Current. Apart from Murphy et al's study, we are not aware of other published model studies of the Loop Current behaviors that use the ECMWF (or similarly "realistic") forcing. We exclude from considerations models that assimilate satellite data "onto the Loop Current." It would be difficult to separate mechanisms in such models.

[6] Our objective is to identify the environmental forcing(s) that can explain the disparate shedding periods. We are not suggesting, however, that the shedding phenomenon is "predictable." Rather, we think that the phenomenon may be rooted in mechanisms with parameters that are "observable" at Yucatan, though these parameters (e.g., vorticity influx from the Caribbean) are themselves chaotic. Apart from a purely scientific curiosity for the phenomenon, knowledge of the relative importance of these forcings will aid in a more comprehensive design of a hindcast model of the Gulf. Identification of the parameter(s) may lead to a better understanding and perhaps a more accurate prediction of the Loop Current's behavior, especially in combination with satellite data and assimilation techniques.

[7] This paper is organized as follows: section 2 presents the model. Section 3 describes numerical experiments designed to separate effects of winds and Caribbean eddies. Section 4 presents the results. First, we will show that in the absence of wind forcing and Caribbean eddies, the dominant shedding periods are 9–10 months. We will then show that when the model is forced by six hourly ECMWF winds, the shedding period histogram shifts predominantly to shorter periods, some as short as 3 months. On the other hand, when forced by anticyclonic Caribbean Sea eddies, the model histogram shifts to longer periods, some as long as 16 months. In the "wind case," we find that wind-induced transport fluctuations in the Yucatan Channel are forced by similar fluctuations through the Greater Antilles (GA) Passages. Section 5 discusses how anticyclones propagating through the Yucatan Channel from the Caribbean Sea can lengthen the shedding periods. Section 6 is the conclusion.

2. Model

[8] To study the Loop Current's variability, it is necessary to allow a free dynamical interaction between the Gulf of Mexico and the Caribbean Sea. *Oey*'s [1996] model of the Gulf, for example, also includes the northwestern portion of the Caribbean Sea. In the present paper, effects of forcing from the Caribbean Sea and the Atlantic Ocean are to be examined. Oey's model domain is therefore further enlarged to include a portion of the North Atlantic Ocean west of 55°W and from 6°N to 50°N, shown in Figure 3a. Figure 3b shows detailed bathymetry in the southern portion of this

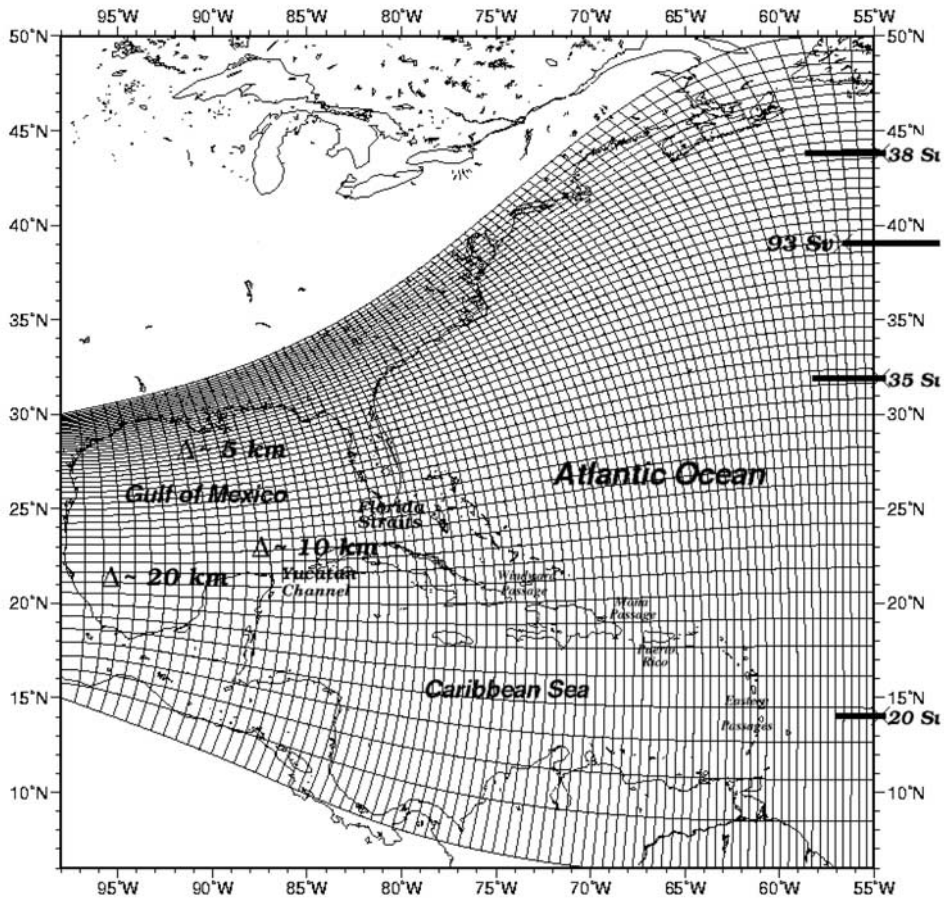

Figure 3a. The model orthogonal curvilinear grid domain encompassing the Gulf of Mexico and Caribbean Sea and portion of the Atlantic Ocean. Grid lines are shown at every seventh grid point. The approximate distribution of grid sizes in the Gulf is indicated, and there are 25 sigma levels in the vertical, with vertical grid sizes less than 5 m near the surface over the deepest region of the Gulf (~3500 m). Time-independent inflow and outflow transport profile, as a function of latitude (y), is specified across the 55°W, as shown schematically.

domain, including the Gulf of Mexico and the Caribbean Sea. The model is based on the primitive equation POM [*Mellor*, 2002], as described in more detail by *Oey and Lee* [2002]. Time-independent total transports are specified at 55°W according to *Schmitz* [1996]. Except for one experiment in which we assimilate sea surface height anomaly from the satellite, the steady transports effectively filter out propagating signals from the region east of 55°W. These transports determine the two-dimensional depth-integrated velocities at the open boundary and are meant to account for the large-scale transports (windcurl + thermohaline) through 55°W. We will for convenience refer to experiments that specify only these transports as "no-wind experiments," though in fact the 55°W transports already include in part a windcurl-driven portion from east of 55°W. The open boundary conditions are a combination of these transport specifications along with radiation and advection as detailed by *Oey and Chen* [1992]. For example, the temperature and salinity fields are advected using one-sided difference scheme when flows are eastward (that is, outflow), and are prescribed from either the annual mean or monthly temperature and salinity from the Generalized Digital Environmental Model (GDEM) climatology [*Teague et al.*, 1990] when flows are westward. These open boundary specifications also set the baroclinic structure, which in the present case is largely geostrophic through the thermal wind balance. All fluxes are zero across closed boundaries. At the sea surface, heat and salt fluxes are zero, but momentum flux (wind) is nonzero in some experiments (next section).

[9] The model grid spacing is $\Delta \approx 10$ km in the northwestern Caribbean/Yucatan Channel and $\Delta \approx 5$ km in the eastern and northern Gulf of Mexico. There are 25 vertical sigma levels with finer resolution over the upper and lower 500–1000 m of the water column [*Oey and Lee*, 2002]. Appendix A gives an estimate of the so-called sigma level pressure gradient error [*Haney*, 1991], which is found to be relatively small (Figure A1). For all experiments, the *Smagorinsky*'s [1963] mixing coefficient is set to 0.1, and the ratio of (horizontal) diffusivity to viscosity is set to 0.1.

3. Process Study Numerical Experiments

[10] *Murphy et al.*'s [1999] experiments suggest that winds and propagating eddies in the Caribbean Sea can

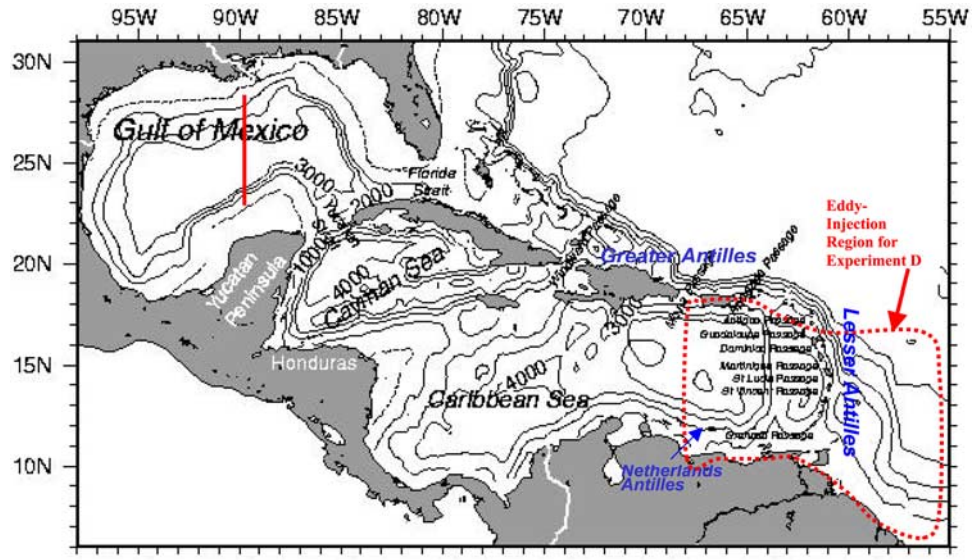

Figure 3b. A detailed locator map and bathymetry of the southern portion of the modeled region that includes the Gulf of Mexico and the Caribbean Sea. Isobaths are 100, 1000, 2000, 3000, and 4000 m. The meridional transect at 90°W in the Gulf is where the model's sea surface elevation is examined to check eddy shedding. The dotted box includes the eastern Caribbean and shows schematically the region where eddies are injected into the model using satellite data in experiment D (see text).

affect Loop Current variability. The *T*/*S* variation at the model boundary at 55°W, which in our model reflects effects in the Atlantic further east, may also affect the results. Five experiments A, B, C, CS, and D are conducted, all have a steady transport specified at 55°W (Table 1). Experiment A specifies only the steady, annual mean *T*/*S* at 55°W and no wind forcing, and Caribbean eddies are not explicitly introduced. Note that although there is no wind forcing for experiment A, the specified transport at 55°W implicitly includes the (steady) windcurl-driven portion from east of 55°W. Experiment B is the same as experiment A, except that a time-dependent, monthly varying *T*/*S* is specified at 55°W. Each of these experiments is initialized by *Oey and Lee*'s [2002] 10-year run, and then continued through 16 years (experiment A has a model setup identical to that described by *Oey and Lee* [2002]). In experiment C we specify six hourly ECMWF wind from 1992 through 1999. It is initialized from the eighth year of experiment B. "Wind effects" will mean motions produced by ECMWF winds specified over the model domain. They are not meant to include the windcurl-driven portion of the transport specified at 55°W. It will be seen that experiment C contains a wider range of shedding frequency than other experiments. To obtain more stable eddy shedding statistics, we extend experiment C by repeating the 1992–1999 ECMWF wind. The extended runs may be taken as twin experiments with different initial conditions. Three such extensions are conducted for a combined total of 32-year time series.

[11] We also conduct experiment CS, which specifies steady wind taken as the time mean of the 1992–1999 ECMWF wind. This experiment is also initialized from the eighth year of experiment B and continued for 16 years. Finally, experiment D sets winds = 0, but eddies are injected in the southeastern portion of the model domain, including the eastern Caribbean Sea (east of 68°W; Figure 3b). The initial field is again from the eighth year of experiment B. The eddy injection is done by assimilating SSH anomaly from satellite into the model, using the assimilation scheme of *Mellor and Ezer* [1990]. This approach uses precomputed surface-to-subsurface correlation coefficients to infer density anomaly as a function of satellite SSH anomaly. Appendix B summarizes the scheme and describes the satellite data. As for experiment C, we also extended experiment D by repeating the 1992–1999 satellite data, but only once for a total of 16 years.

[12] Additional features of the design of experiment D follow. Observations and models [*Johns et al.*, 1990; *Richardson et al.*, 1994; *Fratantoni et al.*, 1995; *Glickson et al.*, 2001; *Fratantoni and Glickson*, 2002; *Heburn et al.*, 1982; *Murphy et al.*, 1999] suggest that rings shed from the North Brazil Current retroflection "collide" with the eastern side of the Lesser Antilles. Remnants of rings then "leak"

Table 1. Model Experiments[a]

Forcing Experiment	Boundary *T*/*S* at 55°W	Wind	Satellite Assimilation
A	steady[b]	...	...
B	monthly[c]	...	...
C	monthly	six hourly ECMWF	...
CS	monthly	mean ECMWF	...
D	monthly	...	SSH anomaly

[a]All experiments have steady transport specified at 55°W, taken from the work of *Schmitz* [1996]. Experiments A, B, CS, and D are for 16 years, while experiment C is for 32 years. Experiments A and B are initialized from the 10-year run of *Oey and Lee* [2002], while the other experiments are initialized from the eighth year of experiment B. (See text for details). Note that the experiments are designed so that only one forcing at one time is changed. The "..." means that the particular forcing is not imposed, i.e., is zero.

[b]Annual climatology.

[c]Monthly climatology.

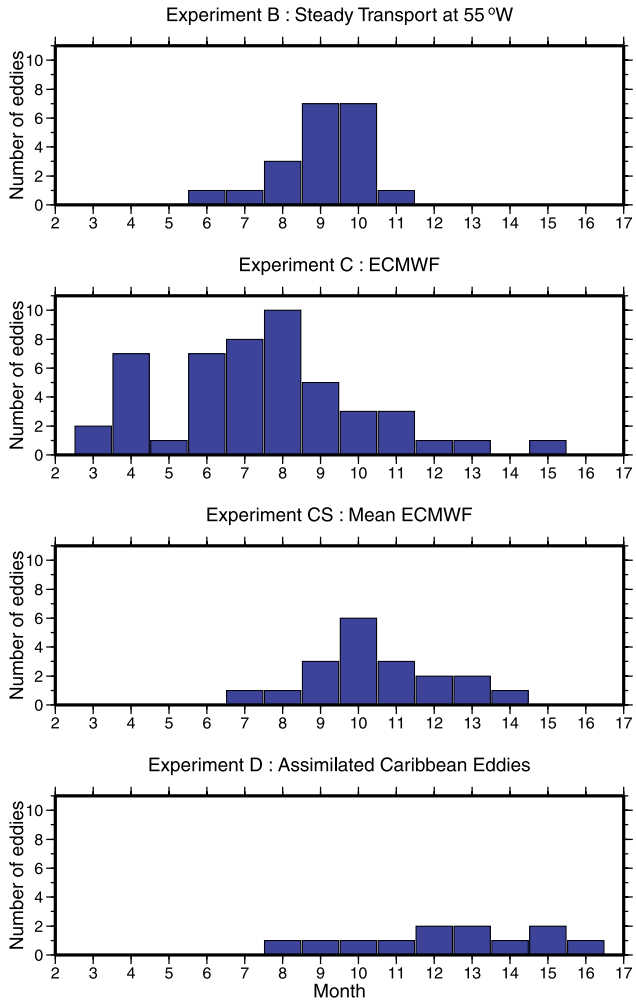

Figure 4. Histograms of Loop Current eddy shedding periods for experiments B, C, CS, and D. The abscissa is time interval in months between shedding, and the ordinate is the number of shed eddies. The result for experiment C is from a 32-year time series, while others are from 16-year time series. (See text for details).

into eastern Caribbean Sea (T. Ezer (personal communication, 2002) also reported such collision in his Atlantic Ocean model [*Ezer and Mellor*, 1997] at ~1/2° resolution. The modeled rings leaked through the Lesser Antilles gaps. However, both Murphy et al.'s and Ezer's solutions may be sensitive to resolution [*Simmons and Nof*, 2002]) and appear to trigger eddy amplification further west. The eddy-triggering and amplification idea seems to be consistent with observations that eddies in the eastern Caribbean Sea are smaller and weaker ''eddy fragments'' of the North Brazil Current rings [*Fratantoni et al.*, 1999; *Glickson et al.*, 2001]. Our model does not include the North Brazil Current and does not simulate the collision process. The model grid sizes in the eastern Caribbean, about 25 km, would also have been too coarse to adequately represent individual Lesser Antilles islands and Passages [*Simmons and Nof*, 2002]. Experiment D is designed to directly inject ''observed'' eddies, which can be fragments or otherwise. Since the injection region includes the eastern Caribbean Sea (Figure 3b), we bypass the very difficult problem of specifying a North Brazil Current and its rings across the model's southeastern boundary at 55°W. The procedure ensures that the injected eddies have reasonably realistic spatial and temporal scales. Once injected (in the specified region shown in Figure 3b), model dynamics dictate the eddy's fate as it traverses westward across the Caribbean basin. On the other hand, our dependence on satellite-acquired data will miss some energetic eddies that have velocity cores below the thermocline and which therefore are not detectable by satellites [*Wilson et al.*, 2002].

4. Results

[13] To display the disparity in shedding periods between different model runs, Figure 4 [cf., *Schmitz*, 2002] shows the histograms of LCE shedding periods for experiments B, C, CS, and D. To double check the shedding period, SSH contours are also plotted (not shown) as a function of time at the meridional transect at 90°W in the Gulf (shown in Figure 3b). These contours confirm Figure 4. The corresponding plot for experiment A is identical to experiment B. Thus the specification of monthly *T*/*S* (rather than annual mean *T*/*S*, as in experiment A) for the boundary at 55°W has little effects on the shedding behavior of the LC. For experiment B (and also for experiment A, same below), Figure 4 shows shedding periods that range from 6 to 11 months, but the 9–10 months periods dominate (14 out of a total of 20 eddies). The tendency for the model Loop Current to shed rings at some preferred or dominant period is similar to the findings of previous model studies [*Hurlburt and Thompson*, 1980; *Sturges et al.*, 1993]. We call this 9–10 month interval the ''natural'' period of eddy separation from the LC [*Hurlburt and Thompson*, 1980]. It is the period at which the model Loop Current would tend to shed eddies in the absence of time-dependent forcing. Figure 5 illustrates a typical example of the eddy separation cycle from experiment B and shows features similar to those in the references quoted above. We treat experiment B as the ''basic'' experiment with two notable characteristics: (1) it has a nearly regular, dominant shedding period of 9–10 months, as mentioned above and (2) the modeled Caribbean Sea is relatively ''quiet,'' i.e., it indicates little eddy activity (Figure 5). Other experiments in Figure 4 show contrasting differences from experiment B. Experiment C displays a wide range of shedding periods from 3 to 15 months. However, the shift (from experiment B) is dominantly to the left of (i.e., shorter than) the natural period. On the other hand, the shifts for experiments CS and D are dominantly to longer periods. We next examine these other experiments, comparing them with experiment B. We will attempt to explain the differences in the LCE shedding histograms for the various experiments as reflected in Figure 4.

4.1. Time-Dependent Wind Case, Experiment C

4.1.1. Mean Transport

[14] The (six hourly) ECMWF wind imposed on experiment C excites motions over a wide range of periods. The spectra (not shown) typically show peaks near the 12- and 6-month periods, but there is also significant energy at shorter periods (~100 days). Figure 6 shows (total) transport time series plots for the Yucatan Channel and the GA Passage (defined as Windward + Mona Passages, *Johns et*

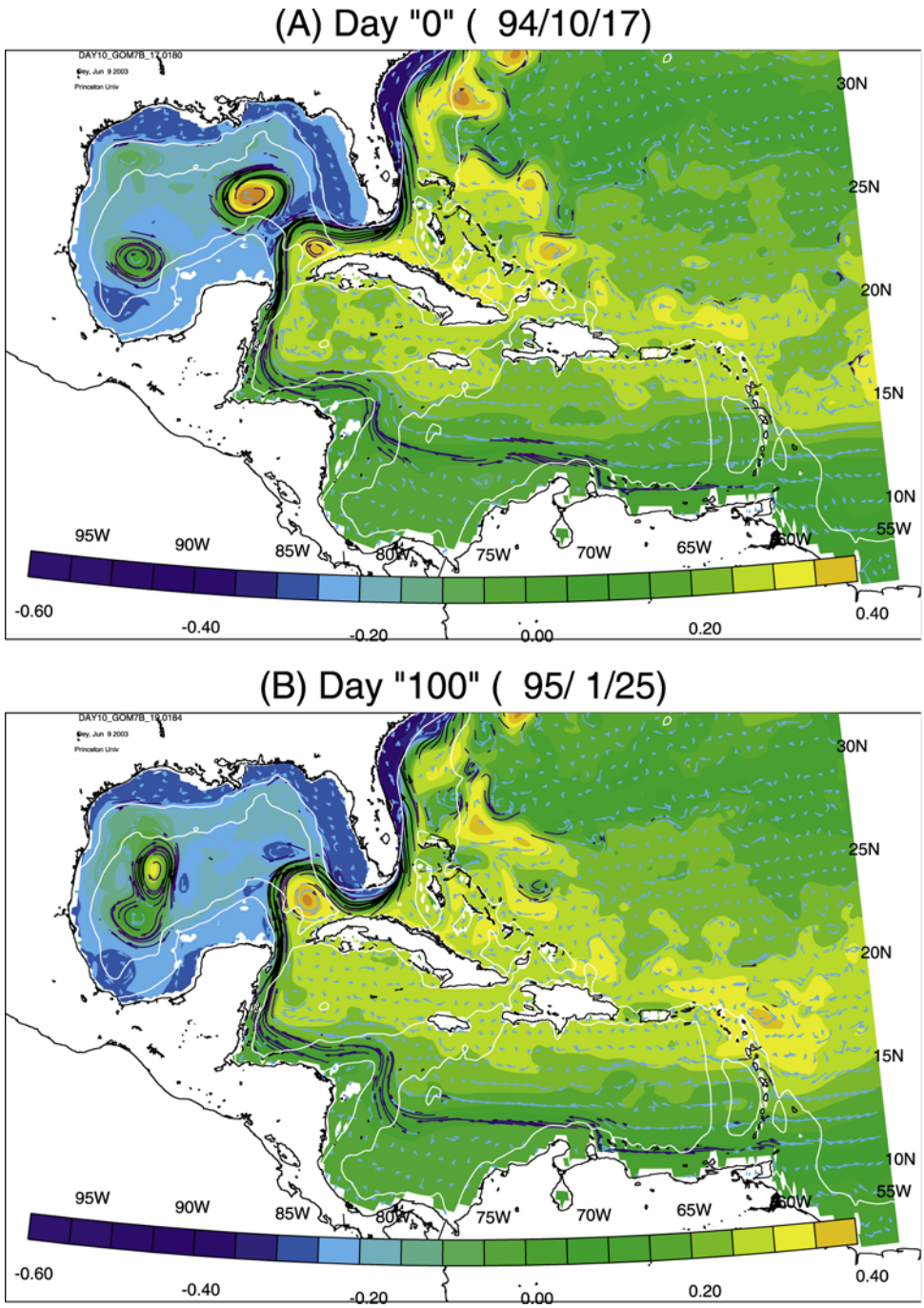

Figure 5. Experiment B: examples of Eulerian trajectories launched for 10 days centered around the indicated date in each figure, and at every eighth grid point at the first sigma level (i.e., surface), superimposed on color image of surface elevation (red for values $\geq$0.4 m, blue <-0.6 m). Colors on trajectories indicate speeds such that [light blue, blue, purple, black] = [<0.25, 0.25–0.5, 0.5–0.75, >0.75] m s^{-1}. Light contours are the 200 and 2000-m isobaths. In terms of days, let (a) be day 0 (17 October 1994) when an LCE has just shed; then subsequent figures are (b) day 100 when the LCE has reached the western Gulf and is merging with an older eddy, (c) day 230 when the merged eddy stalls in the southwestern Gulf and the LC expands northward, (d) day 250 when a small cyclone off the southwestern slope of Florida appears and the LC is on the verge of shedding, (e) day 270 when the cyclone appears to cleave the LC and an eddy is shed, and (f) day 290 when the shed eddy moves west. Note also in all figures the Caribbean Current is a narrow blue-purple belt along the southern basin.

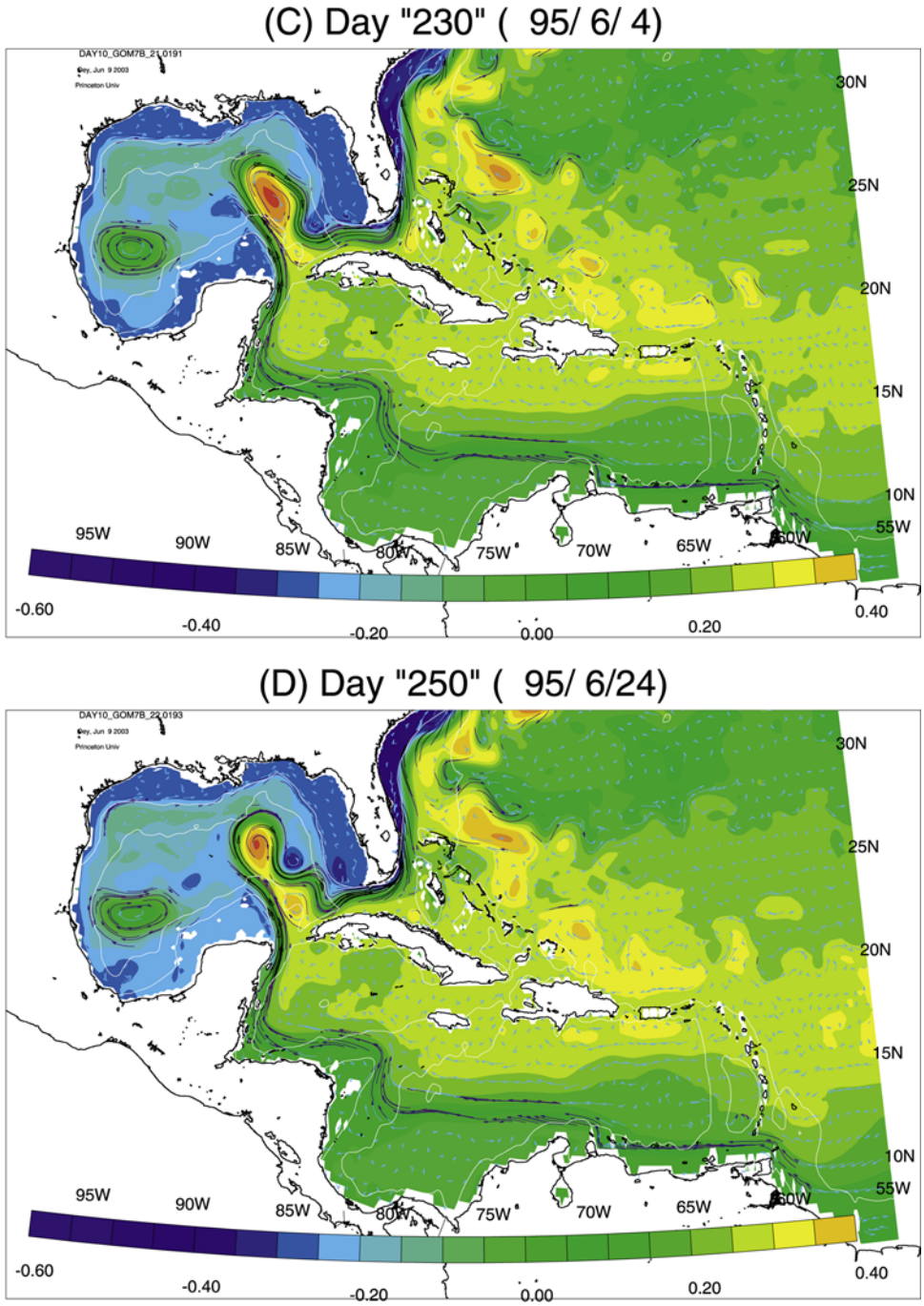

Figure 5. (continued)

al. [2002]). A 10-day running average has been applied to each time series. Figure 6a compares Yucatan Channel transports for experiments B and C and shows that the wind forcing specified leads to an increase in both the mean transport and the amplitude of transport fluctuations. The mean transport is increased by $\langle \delta V_{\mathrm{YUC}} \rangle = 4.4$ Sv, from 22.6 for experiment B to 27.0 Sv for experiment C, where $\langle . \rangle$ denotes a 7-year time mean for experiment C (1993–1999), and this symbol is also used to indicate the mean for the last 7 years of experiment B. The 27 Sv (experiment C) agrees with *Schmitz*'s [1996] estimate. The 22.6 Sv (experiment B) is an underestimate even when compared with the lower value ≈25 Sv from more recent observations [*Sheinbaum et al.*, 2002]. Since the estimated observed transport at 55°W is fixed, it follows that the wind "west of 55°W" is responsible for "channeling" 4.4 Sv into the Caribbean and boosting the Yucatan transport to a value more consistent with those estimated from observations. Figure 7a plots the mean transports lumped into three groups: (1) Yucatan, (2) Greater Antilles, and (3) the remaining (i.e., the Lesser Antilles Passage or LA, which is defined to also include the Anegada Passage; cf. *Johns et al.* [2002]) in experiments B and C. The main difference between the two experiments is the oppositely directed transport through the Greater Antilles. Experiment B has an outflow from the Caribbean to Atlantic Ocean of 4.7 Sv, while experiment C has an inflow

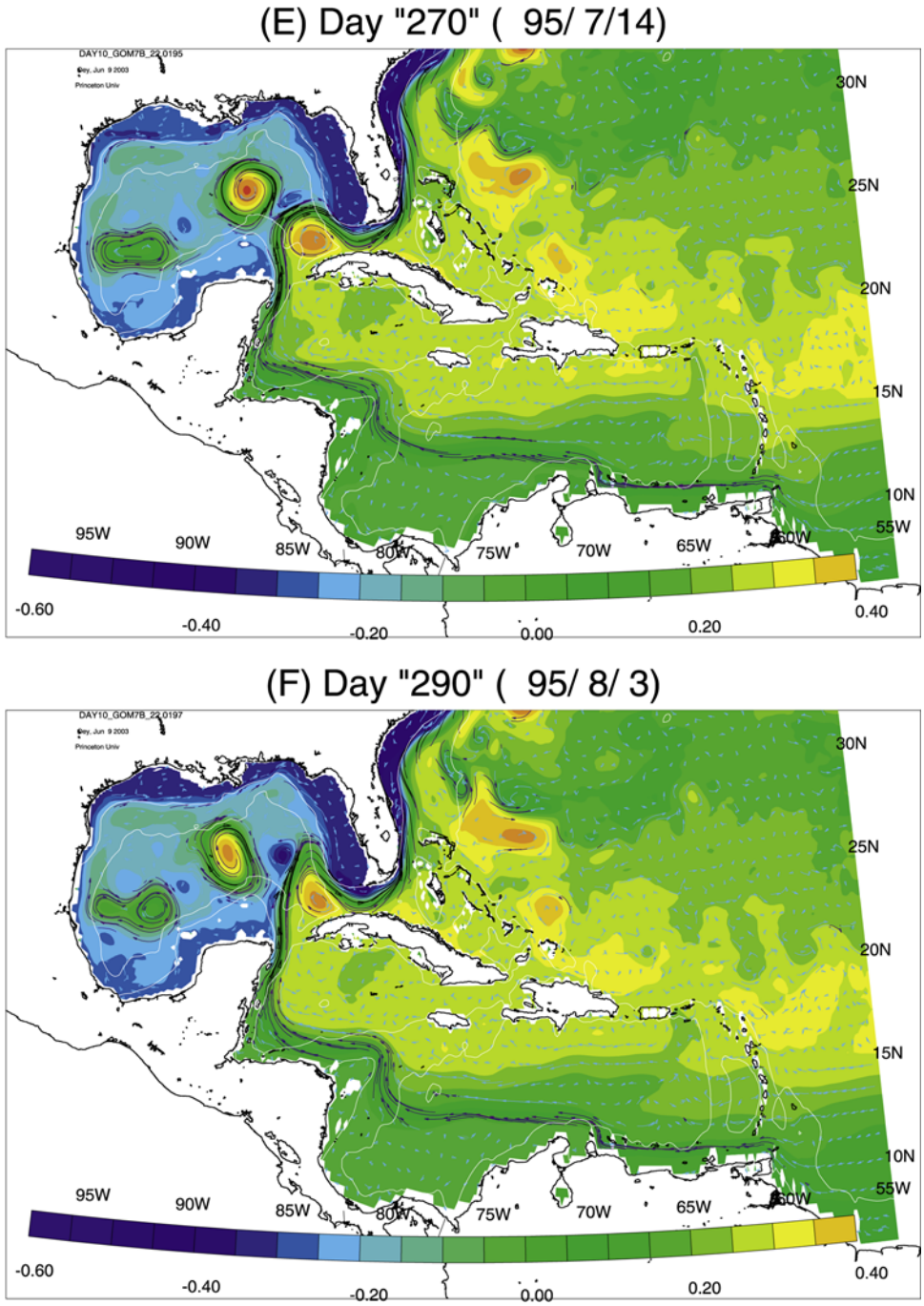

Figure 5. (continued)

of 2 Sv. Though values vary, observations [*Roemmich*, 1981; *Schmitz*, 1996; *Johns et al.*, 1999, 2002] also indicate "inflows" through the Greater Antilles Passage. In their global model, *Murphy et al.* [1999] obtained a $\langle V_{\mathrm{YUC}} \rangle \approx$ 21.5 Sv, and an outflow of 0.8–3 Sv from the Caribbean to the Atlantic Ocean through the Greater Antilles. They attributed these discrepancies with observations to errors in their bottom topography. Their results are similar to experiment B but are different from those of experiment C. The change from the Greater Antilles Passage outflow for experiment B to an inflow for experiment C when the winds are turned on amounts to a "net inflow" of 6.7 Sv into the Caribbean from the Atlantic Ocean. After subtracting the "net outflow" of 2.3 Sv through the LA Passages (see Figure 7a), this net inflow accounts for the 4.4 Sv increase in the Yucatan transport for experiment C. While the (flat bottom) Sverdrup balance does not hold at annual or shorter periods [*Anderson and Corry*, 1985], it should do so for the long-term (7-year) mean. This indeed is the case for experiment C. The mean southward Sverdrup transport was computed across 20°N from the eastern coast of Cuba to the model's open boundary at 55°W to be −3.9 Sv. This value is close to $\langle \delta V_{\mathrm{YUC}} \rangle \approx 4.4$ Sv, the increase in transport through Yucatan caused by wind forcing west of 55°W (i.e., the difference between experiments B and C). Therefore the increased transport depends largely on the strength of the

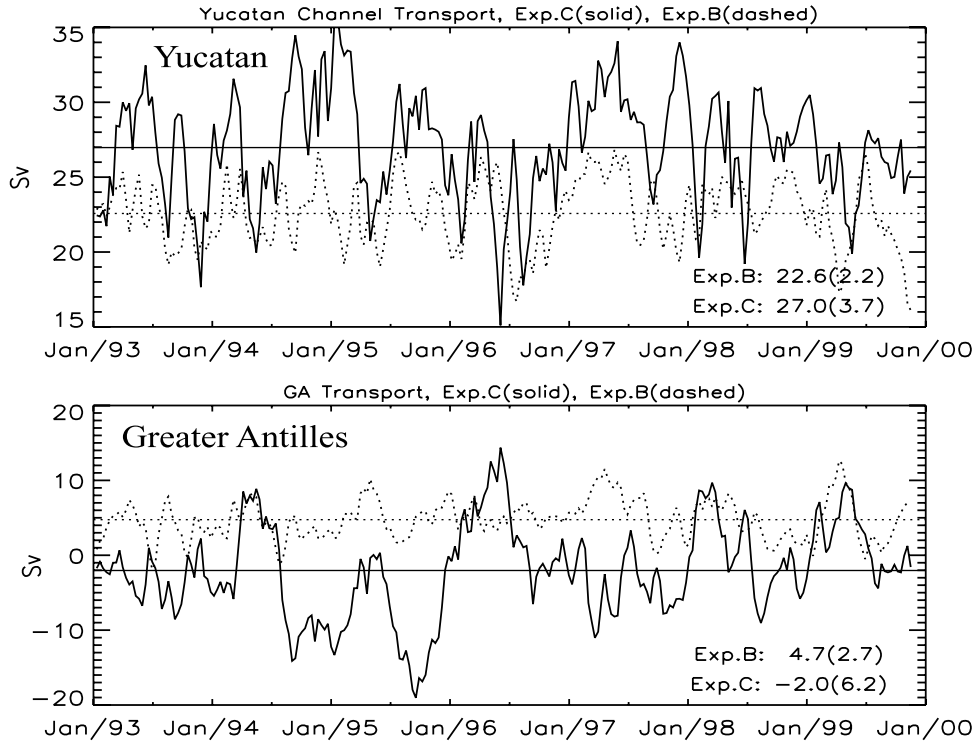

Figure 6. Comparisons between experiment B (without wind; dotted) and experiment C (with wind; solid) of transports in (a) Yucatan Channel and (b) Greater Antilles (Windward and Mona Passages). The indicated numbers in lower right corner of each figure are means and standard deviations for respective experiments. The mean in each case is shown as a horizontal line. All units are in 10^6 m^3 s^{-1} or Sverdrups. The abscissa is dated from January 1993 through December 1999 but is only meaningful for experiment C driven by the ECMWF wind during that period. For experiment B the date is for the convenience of presentation only; it actually represents the last 7 years of the 16-year integration for that experiment.

wind stress curl west of 55°W and north of the Caribbean, i.e., approximately over the southern segment of the Subtropical Gyre west of 55°W.

4.1.2. Transport Fluctuations

[15] Figure 6 shows that experiment C has larger transport fluctuations than experiment B, the difference in standard deviation (SD) is ≈1.5 Sv for the Yucatan transport (experiment B's SD = 2.2 Sv, experiment C = 3.7 Sv). The Yucatan transport in experiment C ranges from 15 to 36 Sv, comparable to observations by *Sheinbaum et al.* [2002]. Not only is increase in the mean Yucatan transport forced by a similar increase in the transport through the GA, as explained previously, so is the corresponding increase in the intensity of the fluctuations. This can be seen in Figure 6b, which compares the GA transport time series of experiments C and B. Without wind (experiment B), SD ≈ 2.7 Sv. With wind (experiment C), SD increases to ≈6.2 Sv. An empirical orthogonal function (EOF) analysis of passage transports in the Caribbean (Yucatan Channel included) indicates that without wind, the mode 1 (57%) transports through Yucatan and GA are "in phase," and both are out of phase with the transports through LA (Figure 7b). In this case, the forcing is through LA, and the responses are through Yucatan and GA, the latter's amplitude being the larger one. With wind, the mode 1 (65%) transports at Yucatan and LA are in phase, with the response at Yucatan now being the more dominant one. Both are now out of phase with the transport through GA (Figure 7b). Note that the solid curves in Figures 6a and 6b are approximately anticorrelated: periods of GA inflow (outflow) roughly correspond to periods of increased (decreased) Yucatan outflow. In this case, the forcing is through GA from the Atlantic Ocean. This may have been anticipated from the previously described role of windcurl over the southern segment of the Subtropical Gyre west of 55°W. However, we now find that flat bottom Sverdrup balance does not hold at these shorter periods. The linear correlation coefficient, γ, between the GA (or Yucatan) transport and windcurl is low (≈0.2 for periods ≈1 year and less, cf. *Anderson and Corry* [1985]). A different proxy is therefore necessary to relate wind effects and flow through the Yucatan Channel.

[16] *Oey* [1996] and *Ezer et al.* [2003] found that fluctuations of the upper 800-m transport at the Yucatan Channel can serve as an approximate indicator of Loop Current's south/north vacillations, including eddy shedding. Figure 8 shows spectral estimates for the upper 800-m transport at Yucatan for experiments A, B, and C. Wind effects can be extracted as the difference solution of the two otherwise identical experiments B and C. The spectrum of the difference transport through GA (δV_{GA}) is also plotted in Figure 8. While δV_{GA} as defined is wind induced, it is poorly correlated with the wind stress curl (see above); it encompasses more complex wind response strongly modified by topography and maybe also eddies in the Atlantic. Experiments A and B show a dominant concentration of energy near the natural shedding period of about

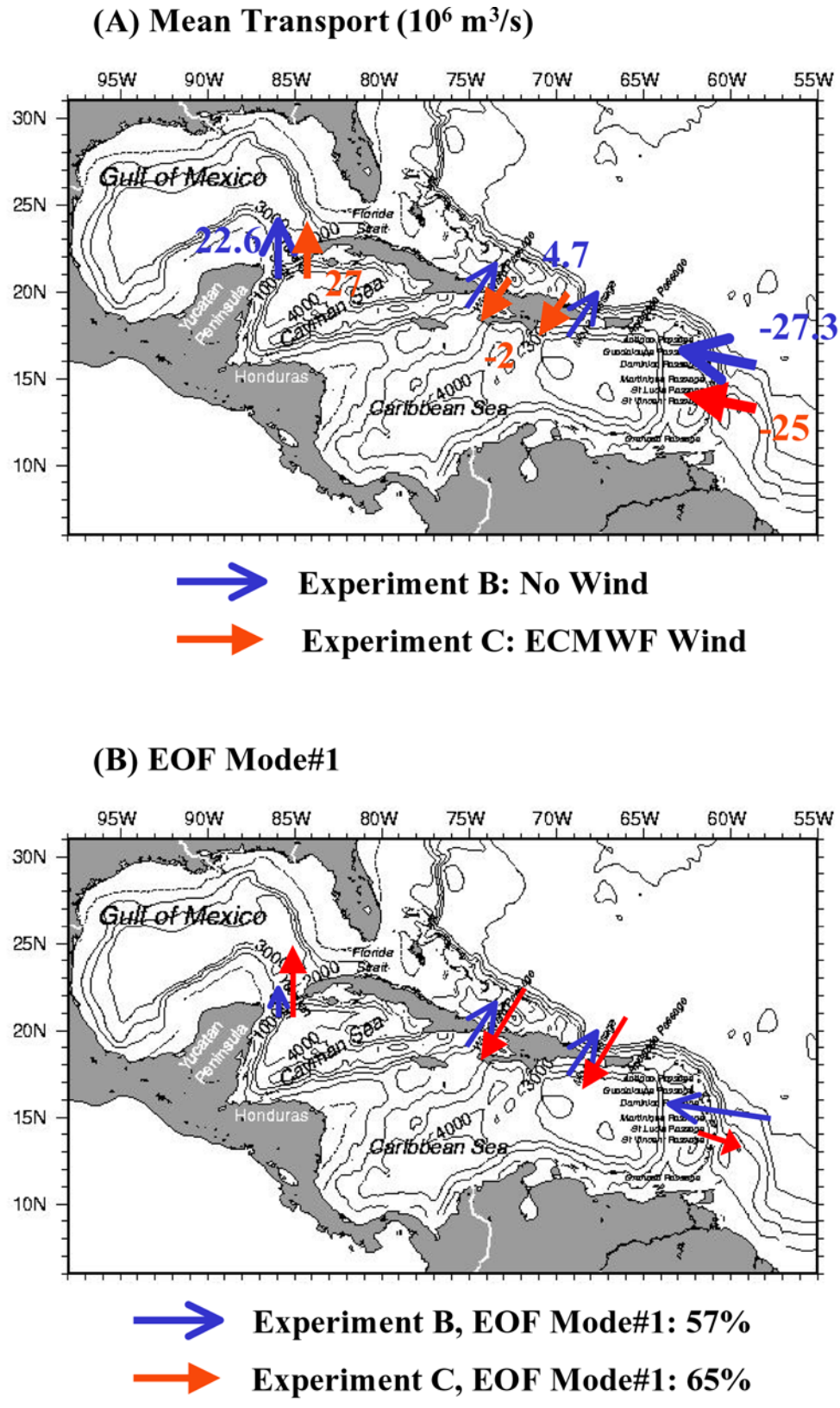

Figure 7. Comparisons between experiments B (no wind; open arrows) and C (ECMWF wind; solid arrows) of (a) the 7-year mean transports (in Sv, 1 Sv = 10^6 m^3 s^{-1}) through Yucatan Channel, Greater Antilles (Windward and Mona Passages), and "lumped" eastern + Anegada Passages and (b) the phasing (i.e., inflow or outflow; size of each arrow is proportional to the corresponding amplitude (arbitrary unit)) of the EOF mode 1 of these channel and passages.

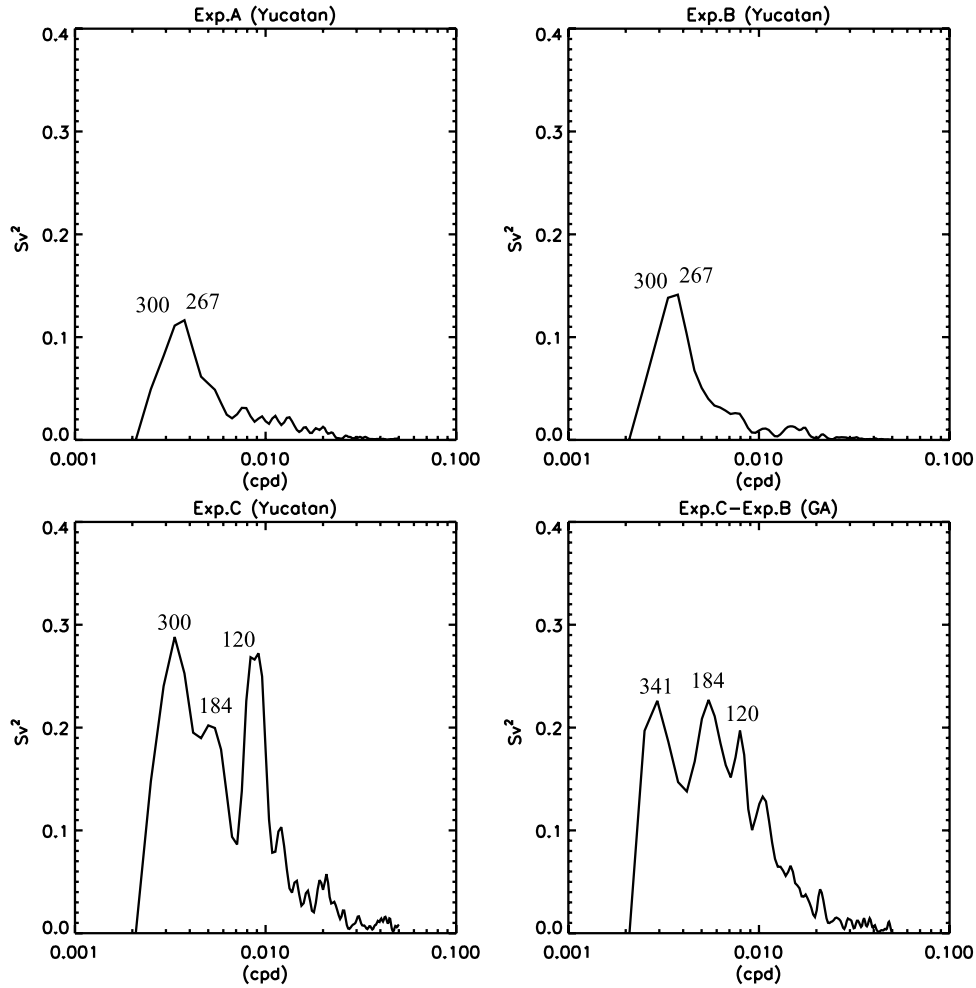

Figure 8. Spectra of the upper 800 m transports in the Yucatan Channel for experiments A, B, and C, and of the difference transport between experiments C and B through the Greater Antilles Passages. Numbers indicate periods in days.

267–300 days described previously (Figure 4). The energy tapers on both sides of these dominant periods. Since the inflow transport into the Caribbean is steady for experiment A or B, the Yucatan transport fluctuations must be local responses to Loop Current shedding events. By contrast, experiment C shows a more broadband energy spectrum at periods that range from 100 to 360 days. In addition to concentration of energy near the natural period, there is now significant energy around 100–120 days. For δV_{GA}, there is no significant peak at the natural period, and the spectrum is also essentially broadband. For experiment C, there is a "dip" in energy around 143 days, corresponding approximately to the low number of shedding at the 5-month period in Figure 4. A similar but less conspicuous dip also exists in the spectrum for δV_{GA}. There is a rough correspondence between the peaks for experiment C at Yucatan Channel and for δV_{GA}. These results are consistent with the previous EOF analysis (Figure 7) that, for experiment C, transport fluctuations through the Yucatan Channel are forced by transport fluctuations through the Greater Antilles. Comparing experiment C with experiment A or B, the tendency for experiment C to predominantly shed eddies at timescales shorter than the natural 9–10 month periods (Figure 4) is attributable to shorter-period transport fluctuations through the Greater Antilles Passages caused by wind forcing. We will later confirm this inference by examining the result for experiment CS when these short-period transport fluctuations through GA are eliminated.

4.1.3. Hispaniola Eddies

[17] Because of the inverse relation between Ekman pumping and the Coriolis parameter, wind stress curls over low-latitude oceans such as the Caribbean Sea can relatively easily spin up eddies. In experiment C, we find one such eddy generation site south-southwest of Hispaniola at approximately (74°W, 17°N), where there exists a localized anticyclonic curl in the wind stress (Figure 9). Both hydrographic and drifter data [*Gordon*, 1967; *Fratantoni*, 2001] indicate anticyclonic circulation in the same region. So potentially the modeled anticyclone is an observable feature. The negative curl is produced by blockage of winds from the northeast by the mountain chains that run almost east/west across Hispaniola and Puerto Rico. Since the wind has a strong steady component, the formation of anticyclone can be approximated by the depression of isopycnals brought about by Ekman downwelling (w_e), assuming a quasi-steady wind stress curl [*Gill*, 1982]. Thus $w_e = (\nabla \times \tau/\rho)/f$, $\approx -10^{-5}$ m s^{-1} for a $\nabla \times \tau/\rho$ value of -4×10^{-10} m s^{-2} from Figure 9b. This "warm lens" then has its pycnocline

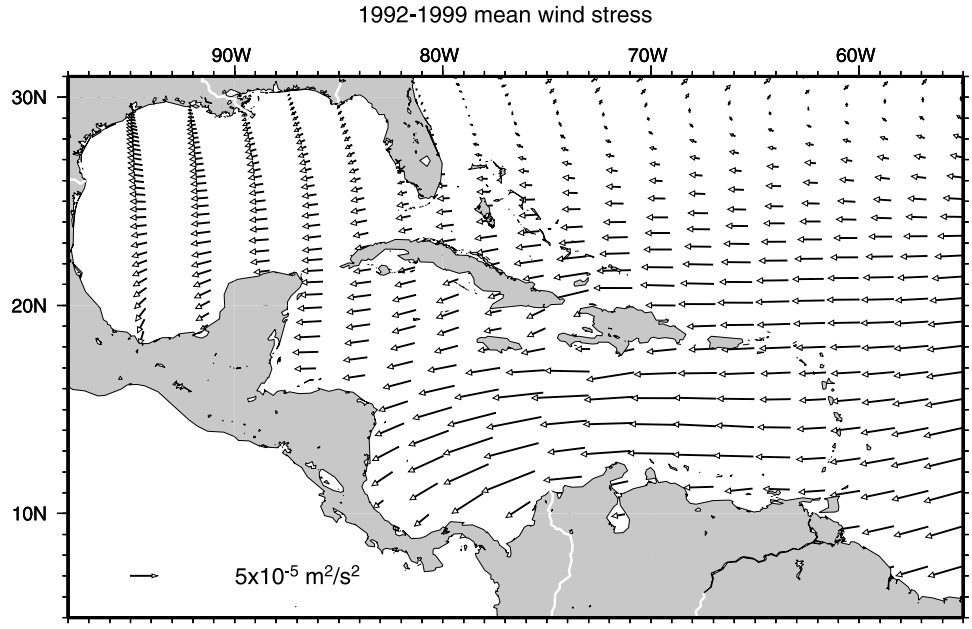

Figure 9a. The 1992–1999 mean wind stress vectors ($m^2\ s^{-2}$; plotted every 10 grid points) derived from the ECMWF wind.

h_e depressed by about 100 m in about 100 days. The lens or eddy also grows to a radius R_e of about 150 km, the scale of the overlying wind stress curl. Taking $\Delta\rho/\rho_0 \approx 10^{-3}$ (from model results), the geostrophic swirl speed near the surface is then $\approx(g\Delta\rho/\rho_0)\nabla h/f \approx 0.3\ m\ s^{-1}$. The β effects become important in a time of about $2R_e/(\beta R_0^2) \approx 100$ days, (note that this is the *Matsuura and Yamagata*'s [1982] timescale. It is the time taken for a (first-mode baroclinic) Rossby wave to traverse the eddy diameter) where $R_0 \approx 40-50$ km. Therefore once formed (in about 100 days), the eddy tends to drift southwestward away from its birth site. The drift is due to the combined action of Rossby wave propagation (westward) and self-advection (southward) as a result of the eddy's interaction with the wake of Rossby wave [*Matsuura and Yamagata*, 1982; *Smith and O'Brien*, 1983]. The eddy is also advected by the generally westward ambient currents. Through this mechanism, anticyclones are (nearly) periodically (≈100 days) formed and shed south of Hispaniola. We will call these anticyclones "Hispaniola Eddies."

[18] Since large anticyclones ($R_e > R_0$) tend to be long-lived [*Matsuura and Yamagata*, 1982], the Hispaniola

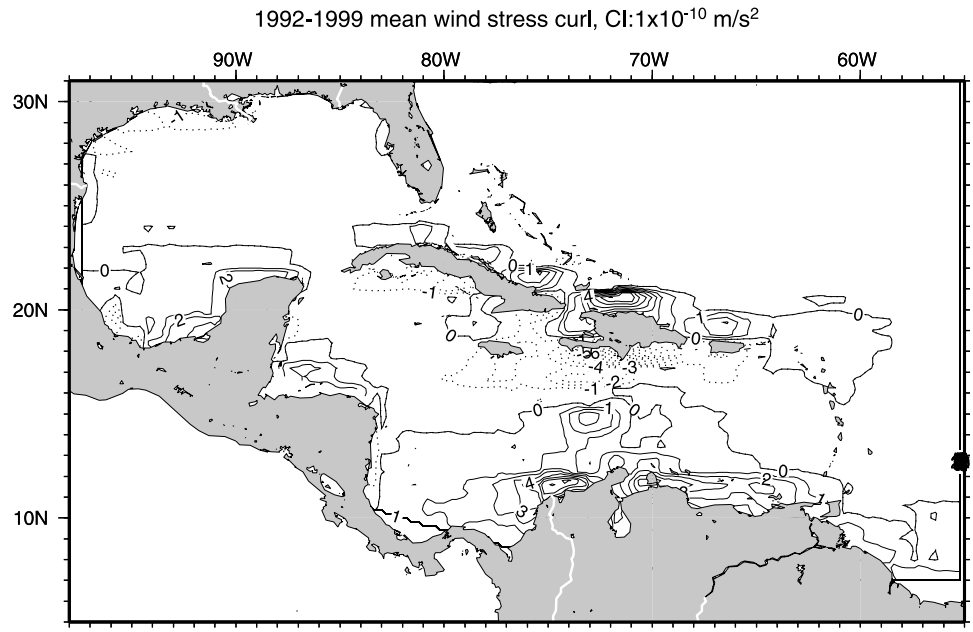

Figure 9b. The 1992–1999 mean wind stress curl (contour interval = $10^{-10}\ m\ s^{-2}$; negative contours are dashed) derived from the ECMWF wind.

eddies continue westward to Yucatan virtually undiminished. Figure 10 shows an example of near-surface currents that illustrate the generation and propagation of Hispaniola eddies. Figure 10a at day "0" (26 November 1996) shows formation of a warm lens southwest of Hispaniola. Note also the train of older eddies into the Yucatan Channel. At day 30 (Figure 10b), the eddy grows to a diameter ≈300 km; its swirl speed increases to 0.25–0.5 m s^{-1}. At day 60 (Figure 10c), the eddy drifts southwestward to south of Jamaica. At day 90 (Figure 10d), the eddy merges with the swift Caribbean Current as it makes a sharp north/northwestward turn over the Nicaragua Rise. At day 120 (Figure 10e), it drifts into the Cayman Basin. And finally, at day 150 (Figure 10f), the eddy arrives at a location just south of the Yucatan Channel. Note that at day 90 (Figure 10d), a new eddy is seen to form southwest of Hispaniola. At day 120 (Figure 10e), this second eddy matures, and at day 150 (Figure 10f) it drifts southwestward. A more detailed analysis for the entire model record indicates that the cycle of eddy formation and drifting repeats at periods 60–130 days. However, these periods densely cluster around a mean of 103 days with standard deviation and skewness equal to 18 days and −0.2, respectively. This simulated period agrees well with the estimate of previous paragraph.

[19] In addition to the above mentioned observations by *Gordon* [1967] and *Fratantoni* [2001], (in section 5, we will present satellite data that appear to also support the existence of Hispaniola eddies) other possible evidence for Hispaniola eddies may be seen in results from the model simulation by *Murphy et al.* [1999]. Though apparently not noted, color snapshots [*Murphy et al.*, 1999, their Plates 2 through 7] of the modeled upper layer thickness and velocity vectors show an east to west band of anticyclones from southwest of Hispaniola to the entrance of Yucatan Channel. However, their anticyclones appear more diffuse than those shown in Figure 10, and other details differ. For example, their anticyclones pass "north" of Jamaica rather than south as seen in Figure 10. It is likely that their eddies are also driven by the wind stress curl field over the Caribbean Sea.

4.1.4. Loop Current Eddy Shedding

[20] Figure 10 also illustrates LCE shedding in experiment C. Figure 10a (day 0) shows a LCE (in the Gulf) that was shed 50 days earlier. During the ensuing 90 days, two Hispaniola eddies from just south of the channel (Figure 10b: day 30, and Figure 10c: day 60) squeeze through and contribute to the northward extrusion of the Loop Current as seen on day 90 (Figure 10d). Shortly thereafter (5–10 days), a new LCE was shed. This newly shed eddy can be seen in Figure 10e (day 120). The time interval between these two eddy separations is ≈4–5 months, shorter than the natural shedding period of 9 ∼ 10 months of experiment B. In this case, the Hispaniola eddies "appear" to shorten the Loop Current shedding period as eddies squeeze through the channel just as the Loop Current is poised for its northward extrusion (i.e., Figures 10a–10c). However, we also find examples in which the Hispaniola eddies simply make an abrupt right-hand turn into the Florida Straits without apparently contributing to the northward extrusion of the Loop Current. These apparently conflicting scenarios arise because experiment C includes eddies from the Caribbean as well as transport fluctuations caused directly by the wind (Figures 6 and 7). Experiments CS and D below isolate effects of Caribbean eddies.

4.2. Steady Wind Case, Experiment CS

[21] As explained above, the Hispaniola eddies are essentially forced by the steady wind stress curl south of Hispaniola and Puerto Rico. Experiment CS therefore specifies a steady wind defined as the 8-year mean of ECMWF from 1992 to 1999. This wind yields Hispaniola eddies similar to those shown in Figure 10 for experiment C. Since this experiment eliminates transport fluctuations through the Greater and Lesser Antilles Passages, it confirms that Hispaniola eddies are not due to these fluctuating transports. Figure 4c shows that the existence and "squeezing through" of these eddies in the Yucatan Channel "lengthen" the LCE shedding periods. Periods of 6 months and less (in experiment C) are now absent, and the 7–8 month shedding interval classes are also reduced to just one occurrence each. The histogram for experiment CS shifts to periods longer than 10 months and as long as 14 months. By comparing experiment CS with experiment B (Figure 4a), which has no eddies in the Caribbean Sea, we have demonstrated that the existence of Hispaniola eddies prolongs the shedding period. By comparing experiment CS with experiment C (Figure 4b), we confirm that short-period eddy separations from the LC in the latter are caused by transport fluctuations due to wind. On the other hand, the three sheddings that one sees in Figure 4 at longer periods of 12, 13, and 15 months for experiment C are likely to be effects of Hispaniola eddies.

4.3. Effects of Eastern Caribbean Eddies (CAREs), Experiment D

[22] The Hispaniola eddies discussed above can also be called "Caribbean eddies". However, in this section, we focus on eddies that originate further east in the Caribbean Sea. These eddies may be a result of "leakage" when the North Brazil Current rings collide with the eastern arc of the Lesser Antilles [*Johns et al.*, 1990; *Richardson et al.*, 1994; *Fratantoni et al.*, 1995, 1999; *Glickson et al.*, 2001; *Fratantoni and Glickson*, 2002]. In experiment D, the eddies are "injected" in the southeastern portion of the model domain, including the eastern Caribbean Sea (Figure 3). Once eddies are injected, their fate as they progress westward into the Yucatan Channel is governed by model dynamics. We find that the sizable eddies (radius R_e ∼ 100 km and larger) that survive to the western Caribbean and Yucatan Channel are predominantly anticyclones. *Matssura and Yamagata* [1982] show that in a timescale of $O(2R_e/(\beta R_0^2))$, ≈100 days for eddy diameters of O(300 km), cyclones rapidly disperse. Thus cyclones would not survive the approximately 1 year of traverse across the Caribbean basin from east to west.

[23] Apart from their origin, the eastern Caribbean anticyclones behave in a similar manner to the Hispaniola eddies, especially after the eddies cross the Nicaragua Rise into the Cayman Basin. Their effects on LCE shedding periods are shown in Figure 4d. The shedding period ranges from 8 to 16 months. When compared with experiment B, it is clear that, as in experiment CS, the shift is toward longer period of eddy separations from the LC. The shedding periods for experiment D also are longer than those asso-

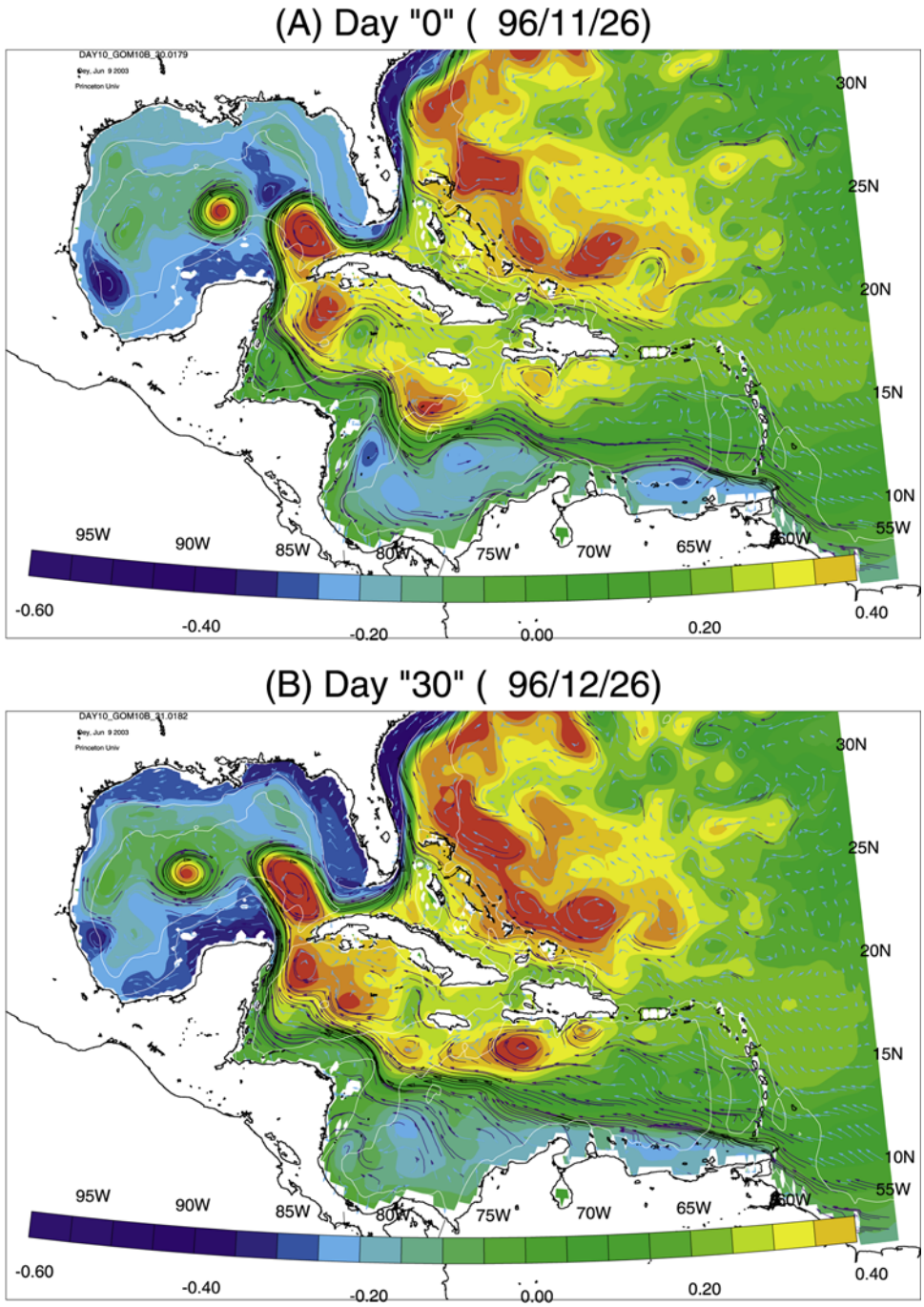

Figure 10. Experiment C: examples of Eulerian trajectories launched for 10 days centered around the indicated date in each figure and at every eighth grid point at the first sigma level (i.e., surface) superimposed on color image of surface elevation (red for values $\geq$0.4 m; blue for values <-0.6 m). Colors on trajectories indicate speeds such that [light blue, blue, purple, black] = [<0.25, 0.25–0.5, 0.5–0.75, >0.75] m s^{-1}. Light contours are the 200- and 2000-m isobaths. In terms of days, let (a) be day 0 (26 November 1996) when an eddy begins to form southwest of Hispaniola; then subsequent figures are (b) day 30 when the eddy has intensified; (c) day 60 when the eddy drifts to south of Jamaica; (d) day 90 when the eddy merges with the Caribbean Current and intensifies as it crosses over the Nicaragua Rise and a new Hispaniola eddy begins to form; (e) day 120 when the eddy moves westward and the new eddy intensifies; and (f) day 150 when the eddy begins to enter the Yucatan Channel and the new eddy drifts to south of Jamaica. These snapshots also illustrate the Loop Current and shedding behaviors as discussed in the text.

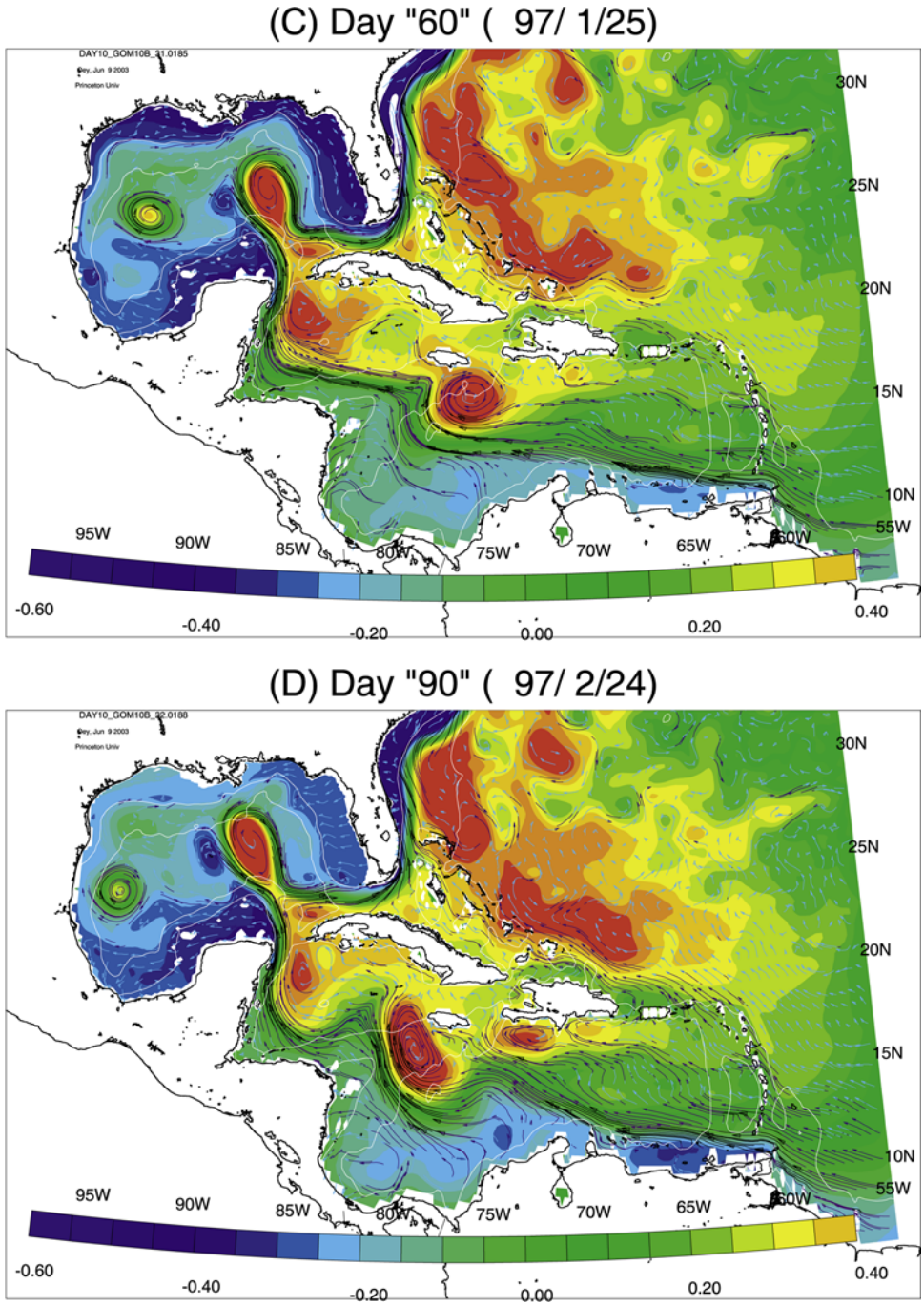

Figure 10. (continued)

ciated with experiment CS, but the number of examples is too small for this difference to be of significance. Experiments CS and D indicate that, in general, the effects of CAREs are to prolong eddy shedding periods.

5. Discussion

5.1. Why Are Shedding Periods Lengthened in Experiments CS and D (With CAREs)?

[24] Since wind induces high-frequency transport fluctuations, it is reasonable that short-period sheddings can occur (as in experiment C). *Hurlburt and Thompson* [1980] found, for example, shedding periods of 7–13 months, when their reduced gravity model was forced by oscillatory (Yucatan) transport with a period much different from the natural shedding period (~9 months). On the other hand, that longer shedding periods should result (as in Experiments CS and D) when the Loop Current is perturbed by CAREs squeezing through the Yucatan Channel is perplexing. Here is one explanation.

[25] The model experiments suggest that the Loop Current and its shedding behavior depend on flow conditions at the Yucatan entrance. In the case of forcing fluctuations by winds and CAREs, the pertinent inflow parameters are the inflow (from Caribbean to Gulf) speed V_c and vorticity ς_0. We may derive a simple relation

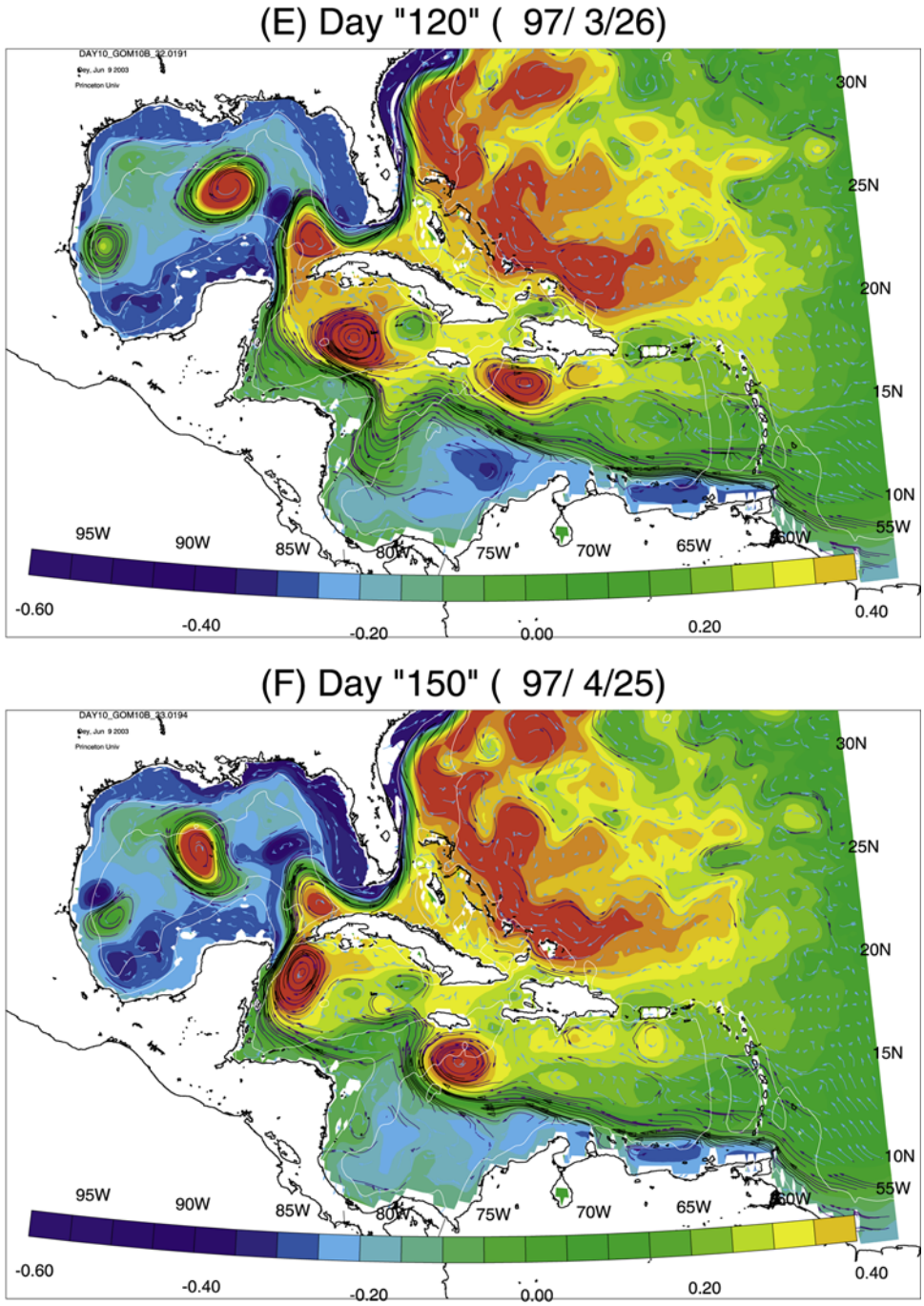

Figure 10. (continued)

between the LC's intrusion distance, b, measured from Yucatan entrance, and V_c and ς_0 following *Reid* [1972] and *Hurlburt and Thompson* [1980], assuming motion in upper layer only. (We know [*Oey*, 1996], of course, that this is not true as lower-layer flows respond to, and perhaps also affect, LC-shedding dynamics. Extending the analysis to include a lower layer is necessary in a future study.) Since inflow speeds are large (>1 m s^{-1}), the timescales of fluctuations (weeks-months) are typically longer than advective timescales (days). We therefore assume that the fluctuations cause the flow to evolve slowly. For convenience, we will also assume a purely south-to-north intrusion at the channel. Conservation of potential vorticity on a streamline then gives

$$b = \zeta_0/\beta + \left[(\zeta_0/\beta)^2 + 2V_c/\beta\right]^{1/2}.$$

This equation is plotted in Figure 11 with "b" a function of ς_0 and for the four indicated values of V_c. Note that for $\varsigma_0 \approx 0$, $\partial b/\partial\varsigma_0 \approx 1/\beta$ and $\partial b/\partial V_c \approx (2\beta V_c)^{-1/2}$. One sees that for a fixed V_c (ς_0), b is a monotonically increasing function of ς_0 (V_c). Thus as $\delta\varsigma_0 < 0$ as for example when a CARE enters the

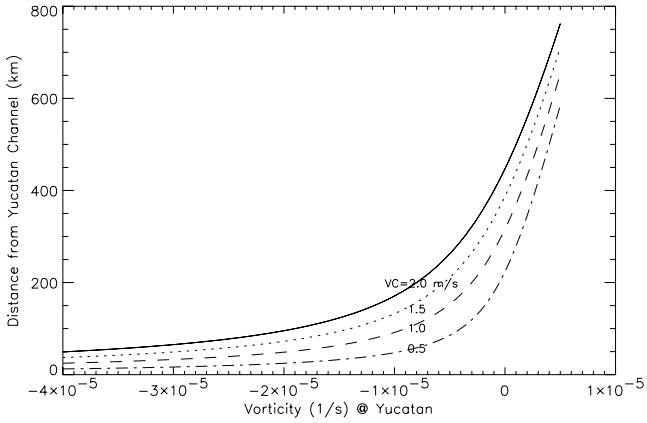

Figure 11. An estimate of Loop Current northward intrusion distance (the ordinate, in km) measured from Yucatan entrance as a function of its inflow (at Yucatan) conditions: relative vorticity (the abscissa, in s^{-1}) and speed V_c (the different curves, in m s^{-1}).

channel (and a fixed V_c is assumed), the Loop Current retracts, $\delta b < 0$. The arrival of a strong CARE ($\varsigma_0 \approx -2 \times 10^{-5}$ s^{-1} or less) can therefore alter an initially near-zero ς_0 such that the LC retracts by O(100 km). A similar retraction would also occur with a decreased inflow V_c. The solution is particularly sensitive to inflow changes near $\varsigma_0 = 0$ (especially for $\varsigma_0 > 0$) when potentially the arrival of a cyclone (anticyclone) would extend (retract) the Loop Current by hundreds of kilometers and similarly for changes in speeds.

[26] When the Loop Current extends (b increases), it is in a more favorable position to shed an eddy [*Hurlburt and Thompson*, 1980] and vice versa when b decreases. We find in general that in experiments with CAREs only, experiments CS and D, the modeled Loop Current tends to stay close to Yucatan. The Loop Current is therefore less prone to shed eddies, and intervals between shedding are prolonged in these experiments.

5.2. Loop Current Eddy Detachment and Reattachment

[27] We find in experiments C, CS, and D that LCEs that are already shed are often reabsorbed into the Loop Current [cf. *Sturges et al.*, 1993]. *Fratantoni et al.* [1998; their Figure 6a] provide an example of this behavior in satellite observations. This eddy detachment and reattachment process occurs on timescales of 1–3 months, shorter than shedding timescales. It may be explained by the response of b (Figure 11) to fluctuating inflow conditions, the V_c, say. As the inflow speed weakens, b retracts and an LCE can detach. The eddy can either be recaptured as the inflow strengthens or is otherwise lost (shed). For example, we find that in experiment C, V_c significantly correlates ($\gamma = 0.5$) with SSH at approximately 150 km north of the channel entrance (see the "cross" in Figure 12) at periods of 1–3 months, a period shorter than the "mean" shedding period of about 7 months (Figure 4b). In other words, in such short time intervals, detached eddies do not have a chance to drift westward and can be recaptured by the subsequent extended Loop Current.

[28] A more complicated response can occur when a CARE arrives. A detached LCE in this case is often recaptured as the CARE squeezes through the channel. Figure 12 gives an example from experiment CS. It shows surface currents colored with local values of ς/f, and superimposed on a color image of SSH. The LCE detaches on 18 August 1999. A CARE arrives at the channel from 18–28 August 1999, carrying with it the white colored trajectories that indicate strong anticyclonic vorticity ($\varsigma/f < -0.4$). The Loop Current makes a tight right-hand turn into the straits of Florida, in accordance with the theoretical prediction that b decreases as $\delta\varsigma_0 < 0$. As the CARE completes its passage through the channel, it interacts with the detached eddy (7–12 September 1999), and the two eddies eventually merge (12–27 September 1999). This scenario is fairly typical of the model output. We summarize it schematically in Figure 13. In Figure 13a, an LCE has just been detached. It begins to drift westward at a speed of about $\beta R_0^2 \approx 1.6$ km d^{-1}, (the drift speed is likely to be slower than βR_0^2, *Hurlburt and Thompson* [1980] and *Nof* [1981]) and the LC turns right into the Florida Straits. In the Cayman Basin, a CARE is approaching the Yucatan Channel at a (model-estimated) northward speed of about 10–15 km d^{-1}. It reaches the channel entrance in about 10–20 days. During this short period, the LCE has not drifted far westward. The CARE squeezes to the right through the channel and "leaks" some of its mass along the northern coast of Cuba. As illustrated in Figure 13b, the two anticyclones interact with each other. There is an eastward induction due to the CARE on the LCE and a westward induction due to the LCE on the CARE. The newly shed LCE can then stall, and the two eddies merge to reform the LC. We find, in the model, that this eddy-capturing scenario typically occurs a few times between two (successful or complete) sheddings. The scenario therefore delays shedding and prolong the shedding period.

5.3. Competing Effects of V_c and ς_0

[29] Using a 2-year long time series of Yucatan Channel Current and density measurements, *Candela et al.* [2002]

Figure 12. (opposite) Loop Current eddy detachment and reattachment, experiment CS: Eulerian trajectories launched for 5 days centered around the indicated date in each figure and from every tenth grid point at the first sigma level (i.e., surface) superimposed on color image of surface elevation (red for values $\geq$0.4 m, blue for values ≤ -0.6 m). Colors on trajectories indicate ζ/f such that black/dark blue through yellow indicate ζ/f from 0 through -0.4 and white for $\zeta/f < -0.4$. Cyclonic trajectories are omitted for clarity. Dark contours are the 200- and 2000-m isobaths. Time interval between figures is 5 days. The first three figures show a LC on the verge of shedding. The LCE is shed or detaches on 18 August 1999. A CARE can be seen to arrive at the channel from 18 to 28 August 1999, carrying with it the white colored trajectories that indicate strong anticyclonic vorticity ($\varsigma/f < -0.4$), and the LC makes a tight right-hand turn into the straits of Florida. As the CARE completes its passage through the channel, part of its mass leaks along the Cuban northern coast (2–7 September 1999). The remaining (main) portion, however, interacts with the shed eddy (7–12 September 1999) and the two eddies eventually merge (12–27 September 1999).

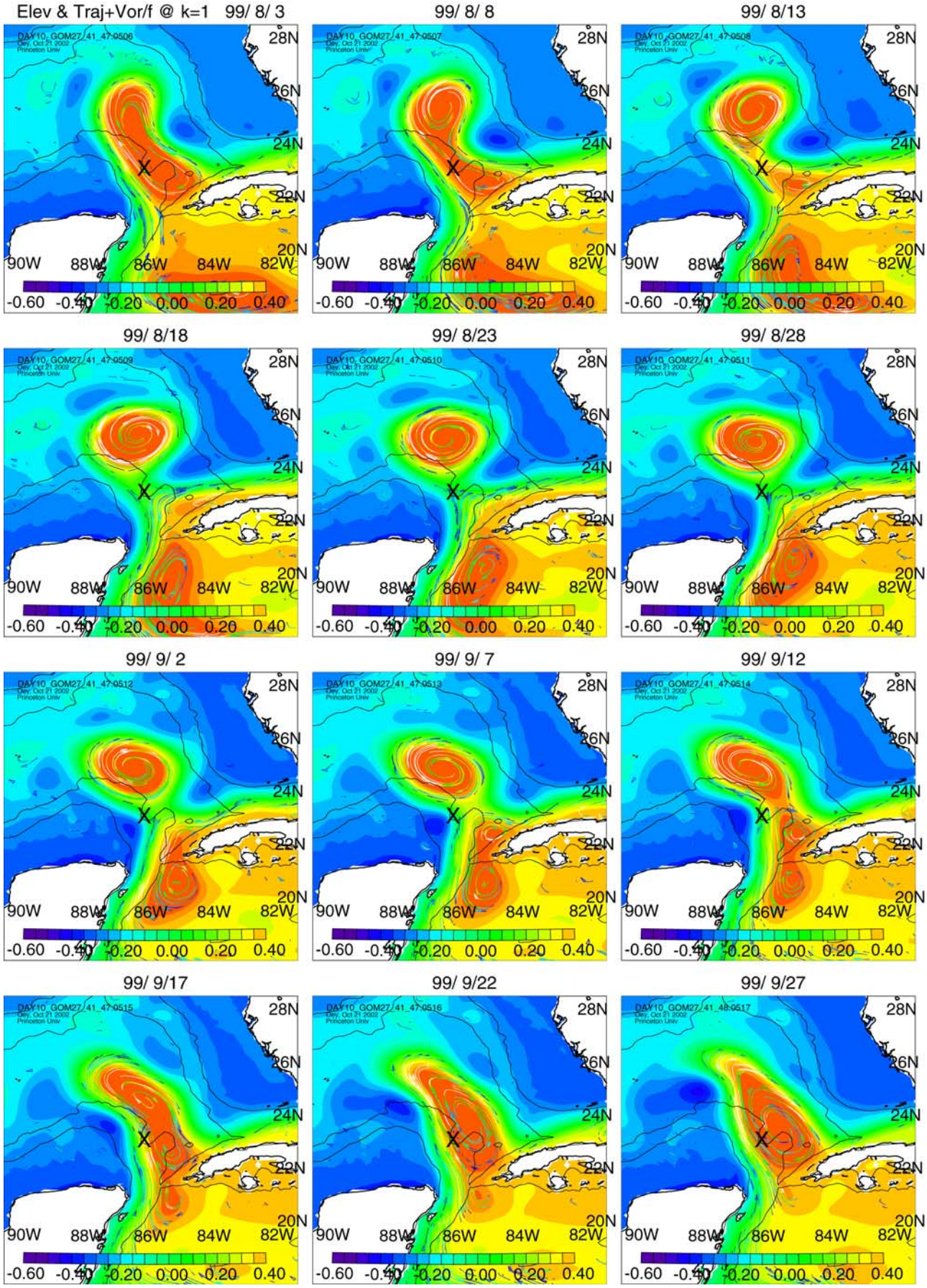
Elev & Traj+Vor/f @ k=1 99/ 8/ 3
99/ 8/ 8
99/ 8/13
99/ 8/18
99/ 8/23
99/ 8/28
99/ 9/ 2
99/ 9/ 7
99/ 9/12
99/ 9/17
99/ 9/22
99/ 9/27
28N
26N
24N
22N
20N
90W
88W
86W
84W
82W
-0.60 -0.40 -0.20 0.00 0.20 0.40

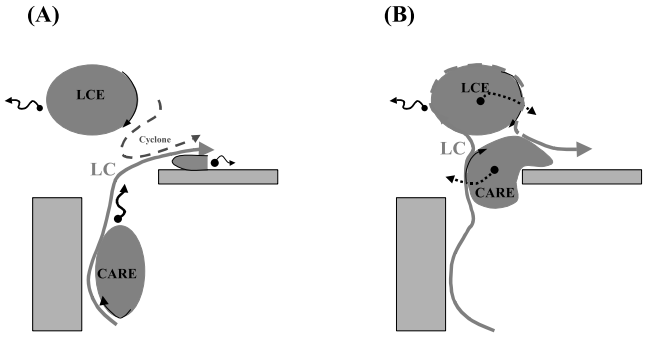

Figure 13. A schematic of interaction between a shed LCE and a CARE squeezing through the Yucatan Channel: (a) the LCE is shed and the CARE is arriving at the channel and (b) the CARE has squeezed through the channel. The mutual induction between the eddies is indicated by dotted arrows and is clockwise tending to "recapture" the LCE. The curvy arrow left of LCE indicates Rossby wave dispersion/propagation.

conclude that the calculated time-dependent potential vorticity flux between the Gulf of Mexico and Caribbean Sea is related to Loop Current intrusion and shedding. Periods of negative cumulative vorticity influx are related to Loop Current intrusion, while periods of positive vorticity accumulation are related to Loop Current retreat and shedding of rings. Though the source of the variability in the vorticity flux was not identified, their finding apparently contradicts what we found with our model. On the other hand, vorticity fluctuations are usually accompanied by inflow current fluctuations. For example, an anticyclone arriving at the Yucatan Channel can trigger an increased current speed. Thus depending on the initial stage in Figure 11, *b* could instead increase, resulting in deeper penetration of the Loop Current into the Gulf. Clearly, these complications can be clarified only through a more indepth model/data analysis and comparison.

5.4. Sensitivity of the Model's Solution to Grid Resolution

[30] The task of checking a model's sensitivity to grid resolution has rarely been done in decadal-scale integrations using eddy-resolving General Circulation Models (EGCMs). More systematic checks have been done with layer models [e.g., *Schmitz and Thompson*, 1993; *Hurlburt and Hogan*, 2000] and with shorter coastal (multilevel) model runs [e.g., *Oey*, 1998]. Insensitivity of the solution to grid resolution would (loosely) indicate numerical convergence [*Chorin*, 1969]. *Richtmyer and Morton* [1957] and *Isaacson and Keller* [1966] give a strict definition of convergence and how it relates to consistency and stability of numerical schemes). The check is useful even if it is limited to just one experiment and one particular aspect of the physics. Appendix C describes such a check. We found significant differences for the modeled velocity profiles (Figure A1) at Yucatan for $\Delta = 20$ km [*Oey*, 1996] and $\Delta \approx 10$ km (experiment C). However, differences in the profiles between $\Delta \approx 10$ km and an otherwise identical doubled resolution experiment, $\Delta \approx 5$ km, are small. Since forcing at Yucatan is of paramount importance in determining the LCE shedding characteristics, we find that the doubled resolution experiment yields a shedding histogram that again shifts toward shorter periods, virtually identical to the corresponding one for experiment C (cf. Figure 4).

5.5. Hispaniola Eddies: Satellite Evidence

[31] The Hispaniola eddies are robust model features. We previously mentioned *Gordon*'s [1967] dynamic height and also *Fratantoni*'s [2001] drifter data. Both indicate anticyclonic recirculation from southwest of Hispaniola to south of Jamaica. However, these are static pictures. Here we examine satellite data. Figure 14 compares RMS values based on satellite-acquired SSH data (Figure 14a), from experiments C (Figure 14b) and CS (Figure 14c). Both model experiments show a band of active SSH variability from southwest of Hispaniola to south of Jamaica and the Cayman basin. The similarity in these regions between these two experiments shows that steady wind curl is the dominant forcing for the excitations of eddies. In the satellite

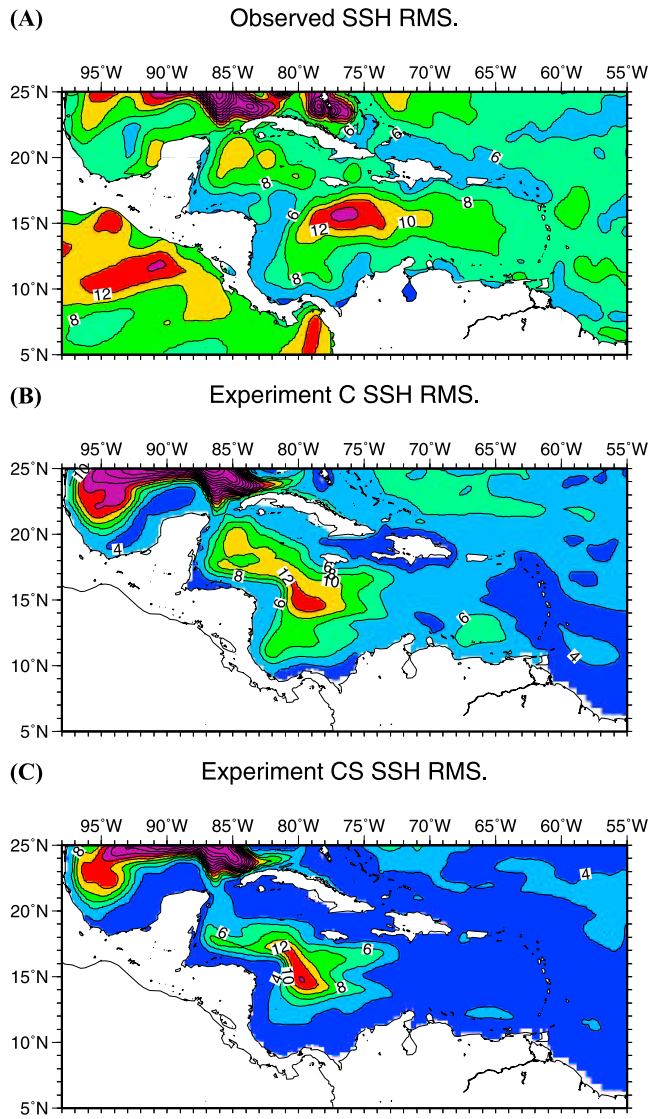

Figure 14. The SSH RMS from (a) satellite SSH anomaly (1992–1999), (b) experiment C, and (c) experiment CS.

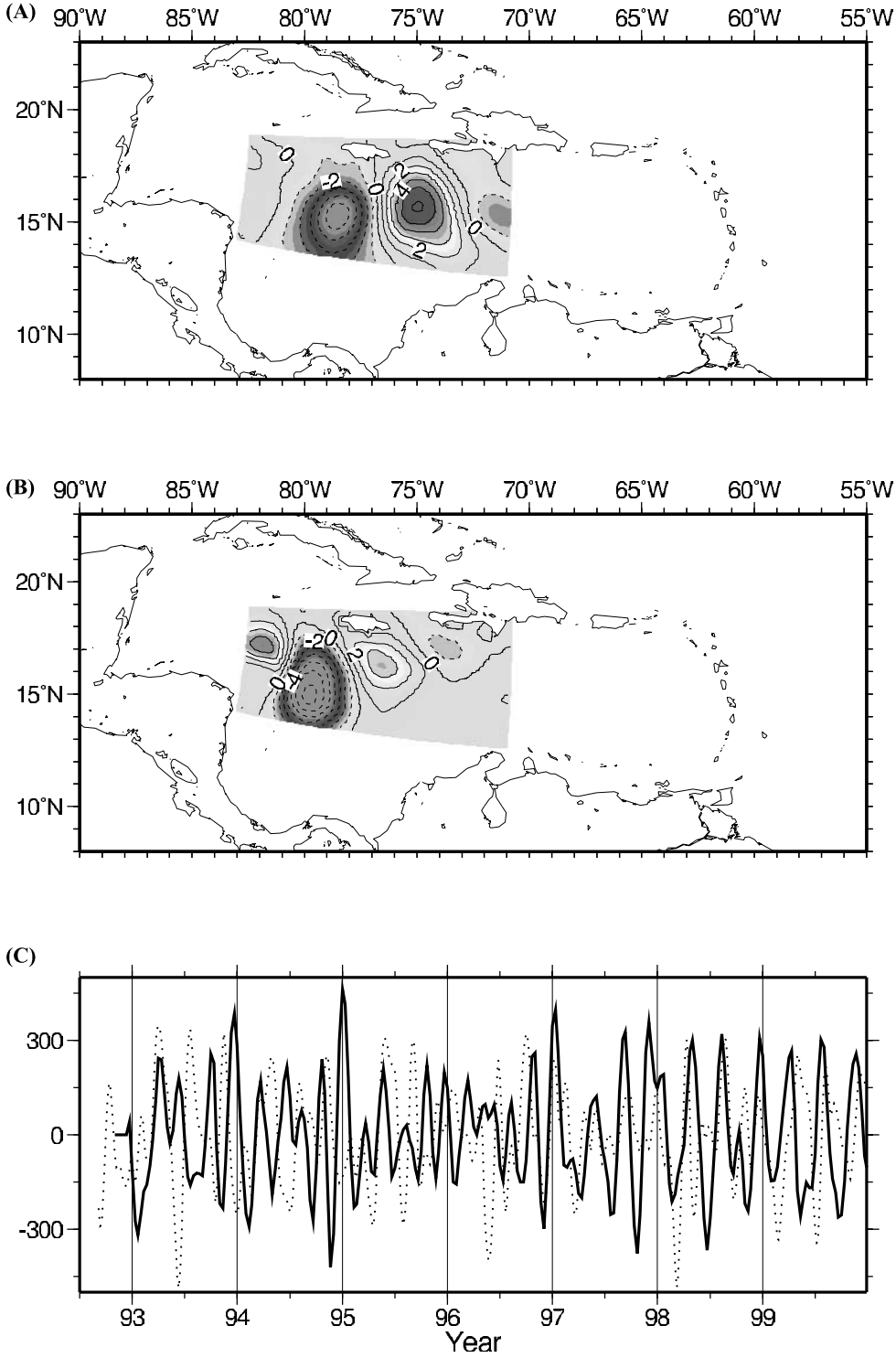

Figure 15. (a) The second EOF mode (20%) from satellite SSH anomaly (1992–1999), (b) the first EOF mode (26%) from experiment CS, and (c) the corresponding time series (solid: satellite; dotted: model). The region is southwest of Hispaniola, as shown. The time series for model has been phase-shifted by π in order to show the similarity in periods of fluctuations between the model and satellite. Both show periods $\approx$100 days.

data, this band of increased eddy activity extends more to the east. It is clear, however, that the dominant westward increase begins south of Hispaniola. EOF analyses indicate that the first satellite mode (31%) is annual. The second satellite mode (20%) is compared with the model's first mode (26%; from experiment CS) in Figure 15 (the model does not have an annual mode). While there are differences in the detailed positions and relative strengths of the modeled and observed modes, both have periods of about 100 days and similar spatial structures. Considering that the

real ocean is a chaotic mix of eddies, the agreement (Figures 14 and 15) in temporal and spatial structure supports the idea that Hispaniola eddies are forced by the wind stress curl. We hypothesize that, in the real ocean, the Hispaniola eddies play an important role in affecting the Loop Current variability, perhaps through the process described in this paper.

5.6. Other Caribbean Characteristics

[32] Comparing experiments C and CS in Figure 14 shows that experiment C has an increased SSH RMS that extends more into the Yucatan Channel, as well as also into the southwest Columbian Basin. There is good agreement between experiment C and the satellite RMS in this southwest basin, and to a lesser extent near the Yucatan Channel. In contrast, experiment CS underestimates the amplitudes. Therefore time-dependent wind forcing (experiment C) is important in these localized regions, probably through the excitation of local basin modes.

[33] On the other hand, even when forced by a comprehensive set of wind products that contain high frequencies, experiment C still underestimates the observed SSH RMS, especially east of ~75°W. This suggests that either the model resolution and physics, or the forcing, or both, are inadequate. Two potentially important forcing mechanisms that we excluded in the present model study are (1) the leakage of North Brazil Current rings through the islands of the Lesser Antilles and (2) in general, perturbations in the Atlantic Ocean east of 55°W. The weaker modeled eddy activity may also be a result of the Caribbean Current not being adequately resolved, with instabilities in this current system, along with smaller-scale eddies, not being simulated.

6. Summary and Conclusion

[34] A variety of numerical experiments were used to identify forcing mechanisms associated with upstream conditions in the Atlantic Ocean and the Caribbean Sea that can affect the transport in the Yucatan Channel and the Loop Current eddy separation process. The wind-driven experiment (experiment C) yields a Yucatan Channel transport: (mean, range) = (27, 15–36) Sv (Figure 6) comparable to that observed. A mean transport of −2 Sv (from Atlantic to Caribbean) through the Greater Antilles Passages is simulated, which is also consistent with observation. These transports are compared with those obtained from a model run in which the ECMWF wind is turned off (experiment B). This latter case yields a weaker Yucatan transport (mean, range) = (22.6, 18–27) Sv, as well as a reversed Greater Antilles mean through flow of +4.7 Sv (i.e., from Caribbean to Atlantic; Figure 7). We show that, in experiment C, the large-scale wind stress (curl) over the southern segment of the Subtropical Gyre west of 55°W is responsible for driving the southward transport (also observed) through the Greater Antilles Passages, and also in forcing the increased transport (mean and variability) through the Yucatan Channel. It should be noted that the amplitude of the model determined low-frequency transport fluctuations in the passages of the Greater Antilles can be huge (Figure 6). We have also shown that the variability in the Yucatan Current is in part driven by wind-induced transport fluctuations through the Greater Antilles Passages (Figure 7).

[35] The model experiments suggest that wind and Caribbean eddy-induced transport and vorticity fluctuations in the Yucatan Channel may explain why the LC sheds eddies at irregular intervals. By comparing experiment CS (steady wind) with experiment C (time-dependent wind), we show that short-period, wind-induced transport fluctuations tend to induce shorter-period sheddings (as short as 3 months; Figures 4 and 8). By comparing experiment CS or experiment D (both with CAREs) with experiment B (no CAREs), we show that CAREs (anticyclones) tend to increase the shedding periods (to as long as 14–16 months; Figure 4). Anticyclonic vorticity at Yucatan tends to retard the northward extrusion of the LC, which explains the prolonged periods. These inferences may explain the wide range of observed periods, 3–17 months. Note that our result only indicates the tendency for the LC to shed or not to shed eddies under certain upstream conditions. It does not imply that the LC eddy shedding is predictable.

[36] We have also identified that LCE detachment and reattachment is caused by a "temporary" (~10–30 days) weakening and then strengthening of the Yucatan Current near the surface. This phenomenon can also be caused by the interaction of a Caribbean eddy (that has "squeezed" through the channel) with an LCE (Figure 12). In this case, an LCE can be "recaptured" by the LC, and the process can prolong the shedding cycle. We have not, however, uncovered the underlying mechanism for this (nonlinear) behavior of the eddy shedding process.

[37] We also find that an anticyclonic wind stress curl southwest of Hispaniola spins up anticyclones, which grow and drift westward into the Yucatan Channel. The period of spin-up, growth, and drift is approximately 100 days. These eddies affect the Loop Current behavior (Figure 10). Satellite data support the existence of these eddies (Figures 14 and 15).

[38] Future studies should seek to understand the dynamics of interaction of Caribbean eddies, Loop Current, and LCEs, probably with more idealized models. Grid resolution in the Caribbean Sea should be improved so that the Caribbean Current can be better resolved and its possible instability and meander processes understood. The future model should also incorporate collision of the North Brazil Current rings with the Lesser Antilles and examine leakage of these rings through "island" gaps. Finally, modeled transports through the Caribbean Passages should be compared with observations [*Johns et al.*, 1999, 2002]. Correct simulations of these transports will be required for a more complete understanding of the dynamical interaction between the Gulf of Mexico and the Caribbean Sea.

Appendix A: The Sigma Level Pressure Gradient Error

[39] We check that the sigma level pressure gradient error [*Haney*, 1991] in the model is not large when compared with the physically meaningful modeled currents. The error is reduced by removing the basin-averaged density distribution (in z only) from the time-dependent density field before evaluating the pressure gradient terms [*Mellor et al.*, 1998]. A 1-year test calculation using an initially level

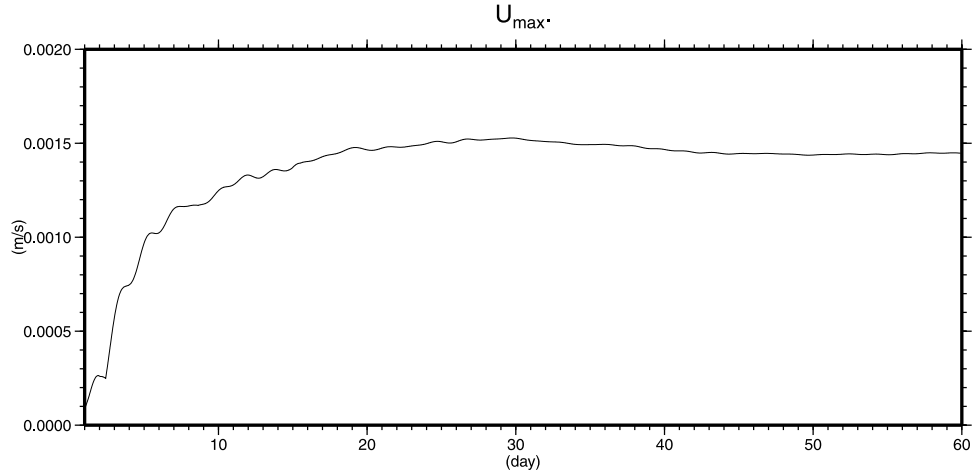

Figure A1. The maximum speed that results from a 1-year test calculation using initially level density field with perturbation: $\rho(z) = \rho_r + \rho'$, where ρ_r = area-averaged and annual mean climatological density, and $\rho' = -0.1$ kg m^{-3} $\times$ exp(z/1000 m) and zero forcing [see *Mellor et al.*, 1998]. For this perturbation, the maximum speed asymptotes to 1.45×10^{-3} m s^{-1} in about 60 days. Only the first 60 days are shown in the plot. The error is approximately proportional to the amplitude of perturbation.

density field with perturbations [see *Mellor et al.*, 1998] and zero forcing was conducted. Figure A1 shows that the maximum error asymptotes to $\approx$0.15 cm s^{-1}, which is relatively small in comparison to, say, the Loop Current speeds $\approx$1 m s^{-1}. Moreover, this maximum occurs off Cape Haterass under the Gulf Stream, removed from the region of particular interest to this study.

Appendix B: Satellite Data Assimilation and Satellite Observations

[40] The satellite data are assimilated into the model following the methodology given by *Mellor and Ezer* [1990]. The model is integrated without assimilation for 8 years, forced by six hourly European Centre for Medium-Range Weather Forecast (ECMWF) winds, and surface heat and salt fluxes. The correlations between SSH anomaly $\delta\eta$ and subsurface temperature and salinity (T/S) are calculated from the model results.

[41] Given the satellite SSH anomaly, $\delta\eta_{sa}$, the model subsurface temperature anomaly δT is calculated as

$$\delta T(x,y,z,t) = F_T(x,y,z)\delta\eta_{sa}(x,y,t), \tag{B1}$$

where the correlation factor is

$$F_T = \langle \delta T \delta\eta \rangle / \langle \delta\eta^2 \rangle, \tag{B2}$$

and the corresponding correlation coefficient is

$$C_T = \langle \delta T \delta\eta \rangle / \left[\langle \delta T^2 \rangle \langle \delta\eta^2 \rangle \right]^{1/2}. \tag{B3}$$

After each assimilation time step Δt_A (=1 day), the model temperature T is replaced by the assimilated temperature T_A:

$$T_A = T + \left[2R_A C_T^2 / \left(1 + 2R_A C_T^2 - C_T^2\right) \right] (T_0 - T), \tag{B4}$$

where R_A is the ratio of Δt_A to the decorrelation timescale Δt_E of the model eddy field ($\approx$30 days), and T_0 is the observed temperature inferred from satellite SSH anomaly, which from equation (B1) is

$$T_0 = \langle T \rangle + F_T \delta\eta_{sa}. \tag{B5}$$

In equation (B5), $\langle T \rangle = T_C$, the climatological mean temperature. The assimilation effect is such that $T_A \approx T_0$ in regions where the correlation is high, but $T_A \approx T$, where the correlation is small. Also, to minimize potential satellite errors near the coast, the assimilation is restricted to regions where water depths are >500 m, thus excluding the shelves.

[42] Satellite altimeter data, Archiving, Validation, and Interpretation of Satellites Oceanographic (AVISO) are obtained from the French Space Agency. The data product was created by merging TOPEX/Poseidon (T/P) and ERS-1&2 altimeter measurements [*Ducet et al.*, 2000]. The combined, intercalibrated altimeter data are interpolated in time and space using a global objective analysis. The length scale of the interpolation varies with latitudes and is about 200 km at midlatitudes. The e folding timescale is set at 10 days in the tropics and 15 days elsewhere. The resulting satellite product has a spatial resolution of 0.25° $\times$ 0.25° and is provided at 10-day intervals. The merged T/P + ERS-1&2 SSH anomaly maps provide reduced and more homogeneous mapping errors than either individual data set, and thus, more realistic statistics. *Fratantoni* [2001] compared AVISO- and drifter-derived kinetic energy and found reasonable agreements. *Wang et al.* [2003] checked the AVISO data against 2-year direct current measurements in the DeSoto Canyon, and found that their first two single-value decomposition [SVD; *Bretherton et al.*, 1992] modes agreed. *Oey et al.* [2003] found that in the Gulf the AVISO data agreed well with those obtained from the Colorado Center for Astrodynamics Research [*Leben et al.*, 2002]. In

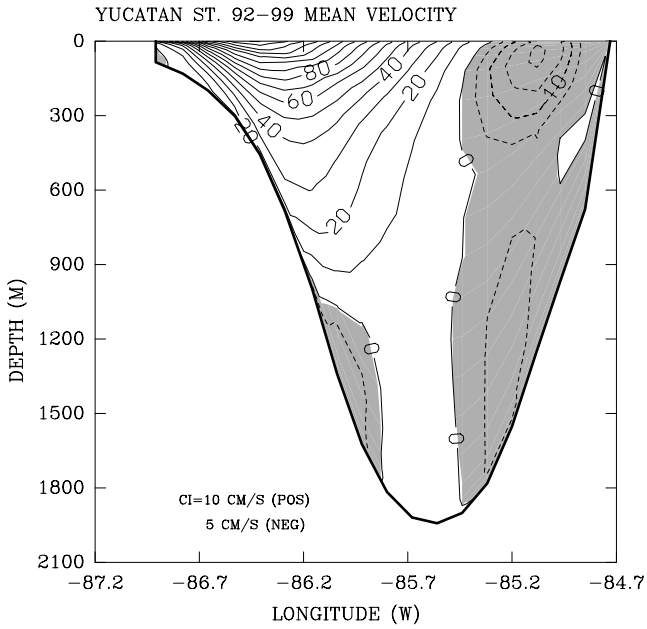

Figure A2. Mean v component velocity normal to the Yucatan Channel as calculated from the model that includes the ECMWF wind (experiment C, Table 1). Shaded region and dashed lines indicate negative values, i.e., from the Gulf into the Caribbean Sea. Contour intervals are 0.1 m s^{-1} for positive and 0.05 m s^{-1} for negative.

this paper, the AVISO data from October 1992 through 1999 are used.

Appendix C: Model Sensitivity to Grid Resolution

[43] The model's orthogonal curvilinear grid has a resolution $\Delta \approx 10$ km in the Yucatan Channel. The grid sizes decrease northward to $\Delta \approx 5$ km in the eastern and northern Gulf of Mexico. The resolution degrades to $\Delta \approx 20$ km in the southwestern corner of the Gulf and also to $\Delta \approx 25$ km in the central and eastern Caribbean Sea, similar to that used by *Murphy et al.* [1999]. Thus in the region of particular interest to this study, the Yucatan Channel and the Loop Current, the resolution is doubled that used by *Oey* [1996; $\Delta = 20$ km] and *Murphy et al.* [1999; $\Delta \approx 25$km]. As a dynamical measure of grid resolution, the ratio, $\Delta/R_0 \approx 0.6$ in the vicinity of the Yucatan Channel, and ≈ 0.7 in the central and eastern Caribbean Sea, where R_0 is the first-mode baroclinic radius of deformation (*Oey* [1998] suggested an empirical criterion that Δ/R_0 should preferably be $\approx 1/3$ or less. The criterion is rarely satisfied in the modeling literature. Most use $\Delta \approx R_0$.). As shown in the text [also cf. *Hurlburt and Thompson*, 1980; *Oey*, 1996], the near-surface inflow velocity through the Yucatan Channel is particularly important in determining the Loop Current behavior. We can take the maximum mean inflow velocity V_{max} as a proxy for the near-surface inflow. Observations yield $V_{max} \approx 1.5$ to 1.75 m s^{-1} (*Pillsbury* [1887] based on direct current measurements, plotted in Figure 5 of *Gordon* [1967], *Schlitz* [1973], *Carder et al.* [1977] based on hydrography) on the western side of the channel, while more recent observations with ADCPs and hydrography by *Ochoa et al.* [2001] and *Sheinbaum et al.* [2002] give a $V_{max} \approx 1.3$ m s^{-1} at about 30-m depth. *Oey* [1996] with $\Delta = 20$ km gives $V_{max} \approx 0.7$ m s^{-1}, which is clearly an underestimate. In the present calculation, $\Delta \approx 10$ km, the experiment that uses the ECMWF winds (experiment C) gives $V_{max} \approx 1.49$ m s^{-1}, as shown in Figure A2. This figure is similar to that shown by *Ezer et al.* [2003], in which we show a variant of experiment C that has also added surface heat and salt fluxes and where a more extensive comparison with observations is presented. A similar profile (as Figure A2) is obtained when we repeat the calculation with an experiments at double the resolution of experiment C; i.e., with $\Delta \approx 5$ km at the Yucatan Channel. We find that $V_{max} \approx 1.50$ m s^{-1} for this double-resolution experiment. The corresponding histogram of LCE shedding period again shifts toward shorter periods, virtually identical to the corresponding one for experiment C (cf. Figure 4).

[44] **Acknowledgments.** L. Y. O. thanks Tony Sturges and Cort Cooper for constructive comments on the first draft of this work. The study is supported by the Mineral Management Service under contracts 1435-01-00-CT-31076. Computing was performed at GFDL/NOAA.

References

Anderson, D. L. T., and R. A. Corry, Seasonal transport variations in the Florida Straits: A model study, *J. Phys. Oceanogr.*, *15*, 773–786, 1985.

Bretherton, C. S., C. Smith, and J. M. Wallace, An intercomparison of methods for finding coupled patterns in climate data, *J. Clim.*, *5*, 541–560, 1992.

Brooks, D. A., and R. V. Legeckis, A ship and satellite view of hydrographic features in the Gulf of Mexico, *J. Geophys. Res.*, *87*, 4195–4206, 1982.

Candela, J., J. Sheinbaum, J. Ochoa, A. Badan, and R. Leben, The potential vorticity flux through the Yucatan Channel and the Loop Current in the Gulf of Mexico, *Geophys. Res. Lett.*, *29*(22), 2059, doi:10.1029/2002GL015587, 2002.

Carder, K. L., A. Fanning, P. R. Betzer, and V. Maynard, Dissolved silica and the circulation in the Yucatan Strait and the deep eastern Gulf of Mexico, *Deep Sea Res.*, *24*, 1149–1160, 1977.

Chorin, A. J., On the convergence of discrete approximations to the Navier-Stokes equations, *Math. Comput.*, *23*, 341–353, 1969.

Cochrane, J. D., *Separation of an Anticyclone and Subsequent Developments in the Loop Current* (*1969*), *Texas A&M Univ. Ocean Stud.*, vol. 2, edited by L. R. A. Capurro and J. L. Reid, pp. 91–106, Gulf, Houston, Tex., 1972.

Ducet, N., P. Y. Le Tron, and G. Reverdin, Global high-resolution mapping of ocean circulation from TOPEX/Poseidon and ERS-1&2, *J. Geophys. Res.*, *105*, 19,477–19,498, 2000.

Ezer, T., and G. L. Mellor, Simulations of the Atlantic Ocean with a free surface sigma coordinate ocean model, *J. Geophys. Res.*, *102*, 15,647–15,657, 1997.

Ezer, T., L.-Y. Oey, H.-C. Lee, and W. Sturges, The variability of currents in the Yucatan Channel: Analysis of results from a numerical ocean model, *J. Geophys. Res.*, *108*(C1), 3012, doi:10.1029/2002JC001509, 2003.

Forristal, G. Z., K. J. Schaudt, and C. K. Cooper, Evolution and kinematics of a Loop Current eddy in the Gulf of Mexico during 1985, *J. Geophys. Res.*, *97*, 2173–2184, 1992.

Fratantoni, D. M., North Atlantic surface circulation during the 1990's observed with satellite-tracked drifters, *J. Geophys. Res.*, *106*, 22,067–22,093, 2001.

Fratantoni, D. M., and D. A. Glickson, North Brazil Current ring generation and evolution observed with SeaWiFS, *J. Phys. Oceanogr.*, *32*, 1058–1074, 2002.

Fratantoni, D. M., W. E. Johns, and T. L. Townsend, Rings of the North Brazil Current: Their structure and behavior inferred from observations and a numerical simulation, *J. Geophys. Res.*, *100*, 10,633–10,654, 1995.

Fratantoni, P. S., T. N. Lee, G. P. Podesta, and F. Muller-Karger, The influence of Loop Current perturbations on the formation and evolution of Tortugas eddies in the southern Strait of Florida, *J. Geophys. Res.*, *103*, 24,759–24,799, 1998.

Fratantoni, D. M., P. L. Richardson, W. E. Johns, C. I. Fleurant, R. H. Smith, S. Garzoli, W. D. Wilson, and G. J. Goni, The North Brazil Current Rings Experiment (abstract), *Eos Trans. AGU*, *80*(17), Spring Meet. Suppl., S179, 1999.

Gill, A. E., *Atmosphere-Ocean Dynamics*, 662 pp., Academic, San Diego, Calif., 1982.

Glickson, D. A., D. M. Fratantoni, C. M. Wooding, and P. L. Ridchardson, North Brazil Current rings experiment: Surface drifter data report, November 1998–2000, *Tech. Rep. WHOI-00-10*, 129 pp., Woods Hole Oceanogr. Inst., Woods Hole, Mass., 2001.

Gordon, A. L., Circulation of the Caribbean Sea, *J. Geophys. Res.*, *72*, 6207–6223, 1967.

Hamilton, P., Lower continental slope cyclonic eddies in the central Gulf of Mexico, *J. Geophys. Res.*, *97*, 2185–2200, 1992.

Hamilton, P., T. J. Berger, and W. Johnson, On the structure and motions of cyclones in the northern Gulf of Mexico, *J. Geophys. Res.*, *107*(C12), 3208, doi:10.1029/1999JC000270, 2002.

Haney, R. L., On the pressure gradient force over steep topography in sigma coordinate ocean models, *J. Phys. Oceanogr.*, *21*, 610–619, 1991.

Heburn, G. W., T. H. Kinder, J. H. Allender, and H. E. Hurlburt, A numerical model of eddy generation in the southeastern Caribbean Sea, in *Hydrodynamics of Semi-enclosed Seas*, edited by J. C. J. Nihoul, pp. 299–328, Elsevier Sci., New York, 1982.

Hellerman, S., and M. Rosenstein, Normal monthly wind stress over the world ocean with error estimates, *J. Phys. Oceanogr.*, *13*, 1093–1104, 1983.

Hernandez-Guerra, A., and T. M. Joyce, Water masses and circulation in the surface layers of the Caribbean at 66°W, *Geophys. Res. Lett.*, *27*, 3497–3500, 2000.

Hurlburt, H. E., Dynamic transfer of simulated altimeter data into subsurface information by a numerical ocean model, *J. Geophys. Res.*, *91*, 2372–2400, 1986.

Hurlburt, H. E., and P. J. Hogan, Impact of 1/8° to 1/64° resolution on Gulf Stream model-data comparison in basin-scale subtropical Atlantic Ocean models, *Dyn. Atmos. Oceans*, *32*, 283–329, 2000.

Hurlburt, H. E., and J. D. Thompson, A numerical study of Loop Current intrusions and eddy shedding, *J. Phys. Oceanogr.*, *10*, 1611–1651, 1980.

Isaacson, E., and H. B. Keller, *Analysis of Numerical Methods*, 541 pp., John Wiley, Hoboken, N. J., 1966.

Johns, E., W. D. Wilson, and R. L. Molinari, Direct observations of velocity and transport in the passages between the intra-Americas Seas and the Atlantic Ocean, 1984–1996, *J. Geophys. Res.*, *104*, 25,805–25,820, 1999.

Johns, W. E., T. N. Lee, F. A. Schott, R. J. Zantopp, and R. H. Evans, The North Brazil Current retroflection: Seasonal structure and eddy variability, *J. Geophys. Res.*, *95*, 22,103–22,120, 1990.

Johns, W. E., T. L. Townsend, D. M. Fratantoni, and W. D. Wilson, On the Atlantic inflow to the Caribbean Sea, *Deep Sea Res., Part I*, *49*, 211–243, 2002.

Leben, R. R., G. H. Born, and B. R. Engebreth, Operational altimeter data processing for mesoscale monitoring, *Mar. Geod.*, *25*, 3–18, 2002.

Matsuura, T., and T. Yamagata, On the evolution of nonlinear planetary eddies larger than the radius of deformation, *J. Phys. Oceanogr.*, *12*, 440–456, 1982.

Mellor, G. L., *User Guide for a Three-Dimensional, Primitive Equation, Numerical Ocean Model* (*Jul/2002 Version*), 42 pp., Prog. in Atmos. and Oceanic Sci., Princeton Univ., 2002. (Available at http://www.aos.princeton.edu/WWWPUBLIC/htdocs.pom/PubOnLine/POL.html)

Mellor, G. L., and T. Ezer, A Gulf Stream model and an altimetry assimilation scheme, *J. Geophys. Res.*, *96*, 8779–8795, 1990.

Mellor, G. L., L.-Y. Oey, and T. Ezer, Sigma coordinate pressure gradient errors and the seamount problem, *J. Atmos. Oceanic Technol.*, *15*, 1122–1131, 1998.

Merrell, W. J., Jr., and J. M. Morrison, On the circulation of the western Gulf of Mexico with observations from April 1978, *J. Geophys. Res.*, *86*, 4181–4185, 1981.

Murphy, S. J., H. E. Hurlburt, and J. J. O'Brien, The connectivity of eddy variability in the Caribbean Sea, the Gulf of Mexico, and the Atlantic Ocean, *J. Geophys. Res.*, *104*, 1431–1453, 1999.

Nof, D., On the beta-induced movement of isolated baroclinic eddies, *J. Phys. Oceanogr.*, *11*, 1662–1672, 1981.

Ochoa, J., J. Sheinbaum, A. Baden, J. Candela, and D. Wilson, Geostrophy via Potential vorticity inversion in the Yucatan Channel, *J. Mar. Res.*, *59*, 725–747, 2001.

Oey, L.-Y., Simulation of mesoscale variability in the Gulf of Mexico, *J. Phys. Oceanogr.*, *26*, 145–175, 1996.

Oey, L.-Y., Eddy energetics in the Faroe-Shetland Channel, *Cont. Shelf Res.*, *17*, 1929–1944, 1998.

Oey, L.-Y., and P. Chen, A model simulation of circulation in the north-east Atlantic shelves and seas, *J. Geophys. Res.*, *97*, 20,087–20,115, 1992.

Oey, L.-Y., and H.-C. Lee, Deep eddy energy and topographic Rossby waves in the Gulf of Mexico, *J. Phys. Oceanogr.*, *32*, 3499–3527, 2002.

Parr, A. E., A contribution to the hydrography of the Caribbean and Cayman Seas, based on the observations made by the research ship "*Atlantis*" 1933–34, *Bull. Bingham Oceanogr. Coll.*, *5*, 110 pp., 1937.

Pillsbury, J. E., Gulf stream explorations—Observations of currents, appendix 8, pp. 281–290, Natl. Ocean Surv., Silver Spring, Md., 1887.

Reid, R. O., A simple dynamic model of the Loop Current, in *Contributions on the Physical Oceanography of the Gulf of Mexico*, vol. 2, edited by L. R. A. Capurro and J. L. Reid, pp. 157–159, Gulf, Houston, Tex., 1972.

Richardson, P. L., G. E. Hufford, and R. Limeburner, North Brazil Current retroflection eddies, *J. Geophys. Res.*, *99*, 5081–5093, 1994.

Richtmyer, R. D., and K. W. Morton, *Difference Methods for Initial-Value Problems*, 405 pp., John Wiley, Hoboken, N. J., 1957.

Roemmich, D., Circulation of the Caribbean Sea: A well resolved inverse problem, *J. Geophys. Res.*, *86*, 7993–8005, 1981.

Schlitz, R. J., Net total transport and net transport by water mass categories for Yucatan Channel, based on data for April, 1970, Ph.D. diss., 107 pp., Tex. A&M Univ., Corpus Christi, 1973.

Schmitz, W. J., Jr., On the world ocean circulation, vol. I, Some global features/North Atlantic circulation, *WHOI Tech. Rep. WHOI-96-03*, 141 pp., Woods Hole Oceanogr. Inst., Woods Hole, Mass., 1996.

Schmitz, W. J., Jr., Notes on the circulation in and around the Gulf of Mexico, vol. I, A review of the deep water circulation, Conrad Blucher Inst. for Surv. and Sci., Texas A&M Univ., Corpus Christi, 2002.

Schmitz, W. J., Jr., and J. D. Thompson, On the effects of horizontal resolution in a limited area model of the Gulf Stream, *J. Phys. Oceanogr.*, *23*, 1001–1007, 1993.

Sheinbaum, J., J. Candela, A. Badan, and J. Ochoa, Flow structure and transport in the Yucatan Channel, *Geophys. Res. Lett.*, *29*(3), 1040, doi:10.1029/2001GL013990, 2002.

Simmons, H. L., and D. Nof, The squeezing of eddies through gaps, *J. Phys. Oceanogr.*, *32*, 314–335, 2002.

Smagorinsky, J., General circulation experiments with the primitive equations, part I, The basic experiment, *Mon. Weather Rev.*, *91*, 99–164, 1963.

Smith, D. C., IV, and J. J. O'Brien, The interaction of a two-layer isolated mesoscale eddy with topography, *J. Phys. Oceanogr.*, *13*, 1681–1697, 1983.

Sturges, W., and R. Leben, Frequency of ring separations from the Loop Current in the Gulf of Mexico: A revised estimate, *J. Phys. Oceanogr.*, *30*, 1814–1818, 2000.

Sturges, W., J. C. Evans, W. Holland, and S. Welsh, Separation of warm-core rings in the Gulf of Mexico, *J. Phys. Oceanogr.*, *23*, 250–268, 1993.

Teague, W. J., M. J. Carron, and P. J. Hogan, A comparison between the Generalized Digital Environmental Model and Levitus climatologies, *J. Geophys. Res.*, *95*, 7167–7183, 1990.

Vukovich, F. M., An updated evaluation of the Loop Currents eddy-shedding frequency, *J. Geophys. Res.*, *100*, 8655–8659, 1995.

Vukovich, F. M., and G. A. Maul, Cyclonic eddies in the eastern Gulf of Mexico, *J. Phys. Oceanogr.*, *15*, 105–117, 1985.

Wang, D.-P., L.-Y. Oey, T. Ezer, and P. Hamilton, Nearsurface currents in DeSoto Canyon (1997–1999): Comparison of current meters, satellite observation, and model simulation, *J. Phys. Oceanogr.*, *33*, 313–326, 2003.

Wilson, W. G., and K. Leaman, Transport pathways through the Caribbean: The tropical origins of the Gulf Stream, *J. Mar. Educ.*, *16*, 14–17, 2000.

Wilson, W. D., W. E. Johns, and S. L. Garzoli, Velocity structure of North Brazil Current rings, *Geophys. Res. Lett.*, *29*(8), 1273, doi:10.1029/2001GL013869, 2002.

Wust, G., On the stratification and circulation in the cold-water sphere of the Antillean-Caribbean basins, *Deep Sea Res. Oceanogr. Abstr.*, *10*, 165–187, 1963.

Wust, G., *Stratification and Circulation in the Antillean-Caribbean Basins, Part 1, Spreading and Mixing of the Water Types With an Oceanographic Atlas*, Columbia Univ. Press, New York, 1964.

H.-C. Lee and L.-Y. Oey, Princeton University, Program in Atmospheric and Oceanic Sciences, Sayre Hall, Forestal Campus, Princeton, NJ 08544, USA. (lyo@princeton.edu)

W. J. Schmitz Jr., Conrad Blucher Institute, Texas A&M Univervsity, Corpus Christi, TX 78412, USA.